Discovering the Dark Side of the Universe with Neutrinos

Dario Lattuada

LNS INFN

University of Catania

PhD Thesis

1. Spervisors: Insolia A., Sapienza P., Coniglione R.

Day of the defense:

Signature from head of PhD committee:

Contents

List of Figures

List of Tables

LIST OF TABLES

1

Introduction

Dark Matter (DM) is a creature of modern cosmology. For over 75 years we have been wondering on its nature. Despite the construction of new detectors and new theories, we only have hints but still don't have the final answer. Anyway, the answer must be around the corner.

One of the most appealing solution to the problem of the Dark Matter is given by Supersymmetry. Under certain assumptions, Supersymmetry elegantly provides a perfect WIMP (Weakly Interacting Massive Particle) candidate for DM. These Supersymmetric WIMPs can accumulate into dense object like planets, stars and heavier celestial bodies and thus undergo annihiliation to produce Standard Model particles, neutrinos included. We will show how these neutrino signals can be evaulated into modern km^3 Čerenkov neutrino telescopes and which limits can be posed on Supersymmetric DM with the future high energy neutrino underwater telescope KM3NeT.

In this work the next Chapter gives a brief overview of Dark Matter and Supersymmetry topics. The third one is devoted to Neutrino Astronomy, with particular interest on KM3NeT project. The fourth Chapter is about Monte Carlo simulation and neutrino spectra from Neutralino annihilations in the Sun. The results and discussion can be found in the last Chapter.

2

Dark Matter and Supersymmetry

Almost all the information we have about the Universe is photon-driven. Most objects are observed because the emit "light", radiation. We are used to observe the sky and link the position of a light spot with matter. For example, many astronomical mass measurements are based on a mass-luminosity relation and this relation proved itself to be right in so many situations that it still sounds strange to believe that a great component of matter is actually *dark* to us.

However, if we are not completely misled by data coming from different approaches, some "invisible" (*dark*) matter does exist. Dark Matter (DM) has a remarkable history, since the 1930s. Many theories were born by observations of local and distant gravitational anomalies, fluctuations in Cosmic Microwave Background (CMB) radiation, and so on. These theories, some of which involving reformulation of gravitational theory, are hard to reproduce without taking into account a bulk of Cold Dark Matter (CDM) component permeating the Universe.

2.1 Evidence on Dark Matter

The first evidence on "missing" mass contribution is historically ascribed to Bulgarian-born, Swiss-national astrophysicist Fritz Zwicky, of the California Institute of Technology in 1933 (1). By applying the virial theorem to the Coma cluster 2.1 of galaxies, he was able to infer the average mass of galaxies within the cluster, finding a value about hundreds times greater than expected from their luminosity, thus proposing that most of the matter was "dark".

Figure 2.1: Coma Cluster - View of the Coma Cluster of galaxies

These calculations were confirmed and improved in the 1970s, when Vera Rubin studied the rotation curves of galaxies (2). Since most of the stellar mass lies within 10 kpc, one would expect that the rotation curve decreases for larger radii, but many observed rotation curves remain flat out to a very large radius.

At large distances from the centre the gravitational potential should be that produced by a central point mass and, in the absence of forces other than gravitation, it should be expected that

$$\frac{GM}{R^2} = \frac{\vartheta^2}{R} \tag{2.1}$$

with G, universal gravitation constant; M, galactic mass; R, distance from the center of the galaxy; ϑ rotation velocity. Hence $\vartheta \propto R^{-1/2}$ (the Keplerian curve).

The observed slopes for Milky Way are shown in Figure 2.2. It was clear that there is matter-related component in the outer region of the Galaxy. The same slope is found on most of spiral galaxies as shown in Figure 2.3.

Another important tool for dark matter observations is gravitational lensing. Gravitational lensing effects arise from the modification on the space-time produced by mass concentration. According to Einstein General Relativity's predictions, gravitational field deflects the photon light path, thus changing the apparent flux and shape

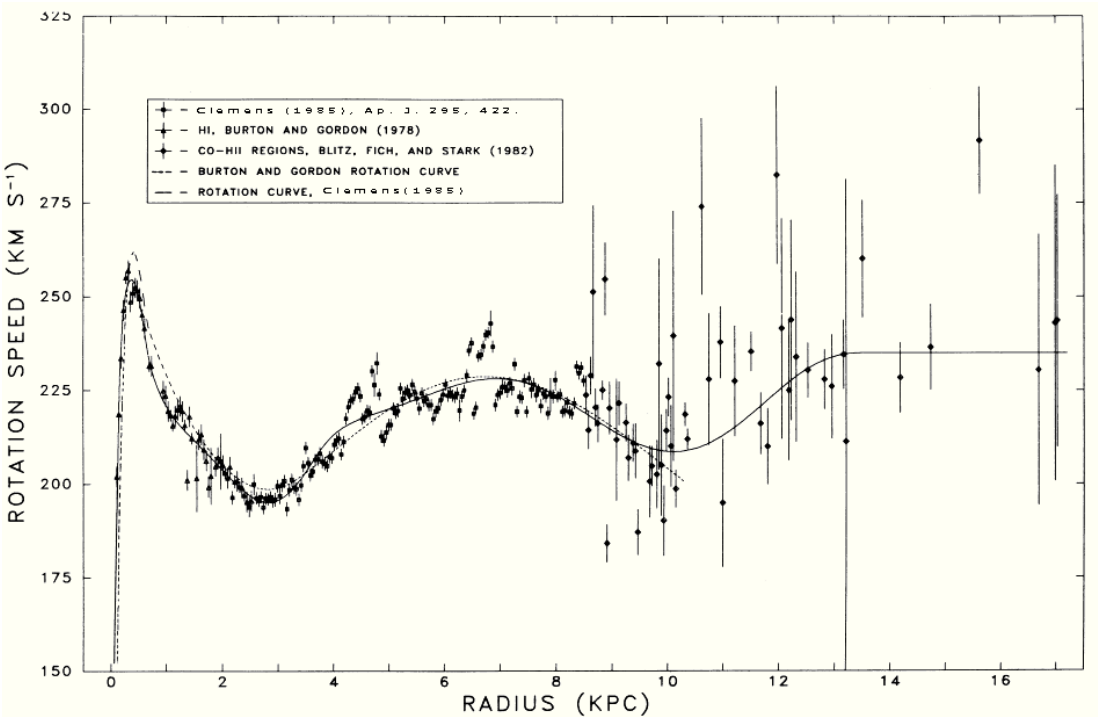

Figure 2.2: Rotational Curves - Rotational Curves of our Galaxy taken from Clemens (1985), Ap. J. 295, 422.

of astronomical sources. By observing gravitional lensing one can in principle infer informations regardless to the matter dristibution, the dynamics or the termodynamics of the system responsible of the *deflecting* gravitational potential. The most successful examples are probably the microlensing experiments, which allowed to set limits on compact dark baryonic objects (MACHOS, Massive Astrophysical Compact Halo Objects like brown dwarves, but also black holes, neutron stars, ...) to constrain their total mass at less than 0.1% of the total *invisible* mass of the Universe.

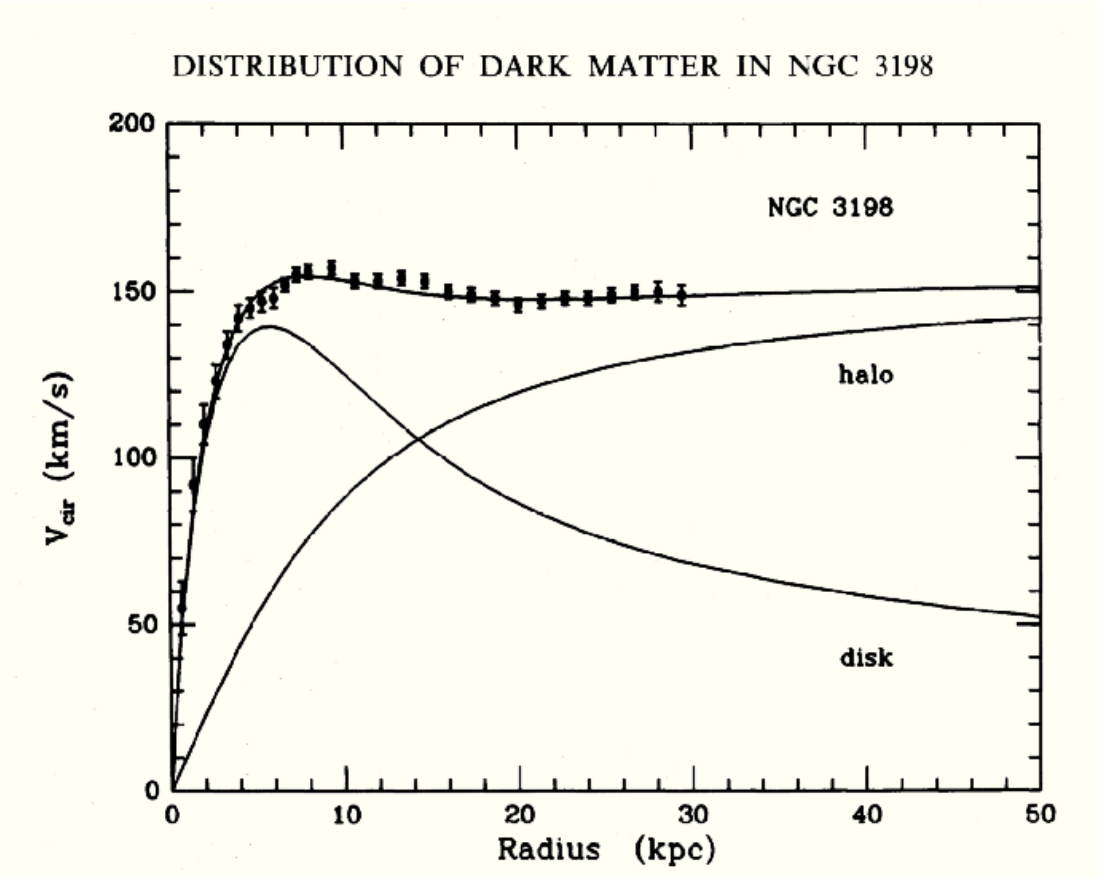

Figure 2.3: NGC3198 Rotational Curve - Rotational Curve of ngc3198 from 2.3.

Beside microlensing, other extragalactic gravitational lensing effects are used in dark matter and modified gravity searches, providing spectacular multiplied, magnified and distorted images with arc-structures as well, coming from distant objects. Assuming General Relativity to be valid, their study showed that:

- Galaxies and clusters of galaxies are dominated by a dark matter component

with mass-to-light ratio of about 10-20 and 100-300 respectively.

- Mass-to-light ratio of galaxies increases with mass and radius, but galactic inner regions appear to be baryon-dominated.

- Mass profiles of galaxies are well described by an isothermal ($\rho \propto r^{-2}$) only in the intermediate zone between bulge and halo.

The simplest model to describe the structure of a dark matter halo is the so-called isothermal sphere. In this model, the probability density function of the three-dimensional WIMP velocity v is given by the Maxwell-Boltzman statistics.

Cosmological N-body simulations and theoretical insight have led to clear predictions for the mass function of dark matter halos that form in the current ΛCDM paradigm (8). On galactic and subgalactic scales, this halo mass function is much steeper than the galaxy stellar mass function, suggesting a complex non-linear relation between the mass of a galaxy and that of its surrounding halo.

Traditionally two different approaches have been used to estimate the DM density function and unfortunately they lead to different results.

The NavarroFrenkWhite (NFW) profile is a radial dark matter density parameterized distribution based on $N - body$ numerical simulations. In the NFW profile, the density of dark matter as a function of radius is:

$$\rho(r) = \frac{\rho_0}{\xi(1+\xi)^2} \tag{2.2}$$

where $\xi = r/r_s$, ρ_0 and r_s are parameters which vary from halo to halo.

However these kind of distributions do not seem to fit well with rotation curve data.

Another approach is the so-called Einasto profile based on the following parameterization:

$$\rho_{DM}(r) = \rho_0 \exp[-(r/r_0)^{1/n}] \tag{2.3}$$

which is in better agreement with data, but actually there's still an open and persisting conflict between predicted and measured central dark matter densities.

Another convincing argument in favour of the dark matter component of the Universe derives from the study of the Cosmic Microwave Background (CMB) radiation, the predicted relic radiation from Big Bang.

After being discovered in 1964 by american astronomers Arno Penzias e Robert Woodrow Wilson, the NASA Cosmic Background Explorer (COBE) provided first accurate measure of a residual signal with perfect blackbody spectrum at 2.726 K, also detecting in 1992 for the first time the fluctuations (anisotropies) in the CMB, at a level of about one part in 10^{-5}. Boomerang and B2K experiments (48) along with COBE's successor, the Wilkinson Microwave Anisotropy Probe (WMAP) provided the most detailed measurements CMB flux, polarization and anisotropies (Figure 2.4) in last years (10).

WMAP's CMB measurements played a key role in establishing the current Standard Model of Cosmology, namely the ΛCDM model (Lambda Cold Dark Matter, Lambda is the cosmological constant, Cold Dark Matter relates to non-relativistic matter).

The ΛCDM model is the most simple model which is in general agreement with observations.

This model describes a Universe dominated by dark energy ($\sim$ 73%) , with a subdominant fraction of dark matter ($\sim$ 23%) and small fraction of baryons ($\sim$ 4%). It is in good agreement with most of large-scale observations as well as CMB anisotropies and supernovae data, in an accelerating Universe framework.

Combined constraints from several measurements on CMB tell us that the Universe is flat. The total energy density in the Universe (in units of the critical density is $\Omega_i = \rho_i/\rho_{crit}$) is $\Omega_{total} = 1.003^{+0.010}_{-0.009}$, and also $\Omega_\Lambda = 0.761^{+0.017}_{-0.018}$, and $\Omega_m = 0.239^{+0.018}_{-0.018}$. Now, measurements of the content of ordinary baryonic matter b yields $\Omega_b = 0.0416^{+0.0019}_{-0.0018}$, leaving us to assume a component of dark matter $W_{DM} = 0.197^{+0.016}_{-0.015}$, about five times larger than the component of ordinary matter.

In order to explain all these observations we can infer two different statements in opposite directions, which require to adopt two different approaches:

- we don't fully understand gravitational interaction ⇒ we need to modify gravitational theory
- we are completely blind to some mass ⇒ we need to introduce new kind of massive *dark* objects

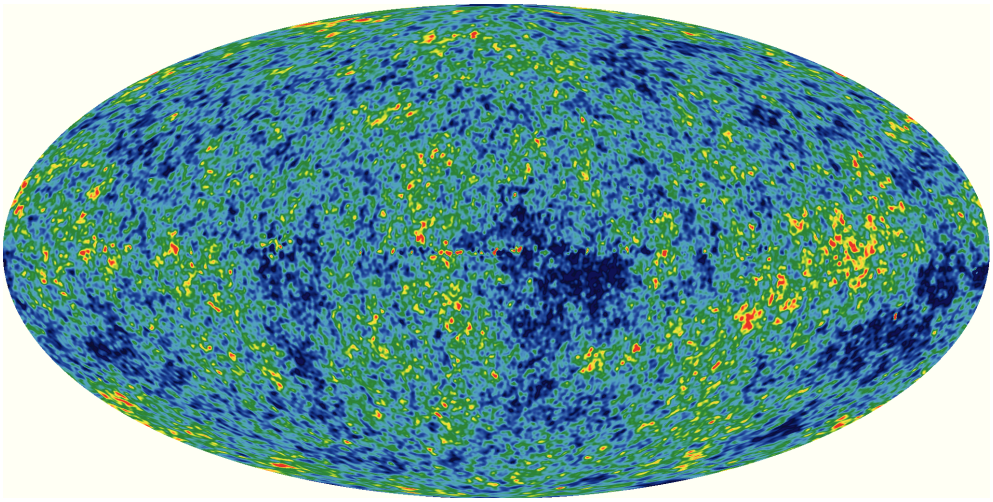

Figure 2.4: WMAP - The detailed, all-sky picture of the infant universe from three years of WMAP data. The image reveals 13.7 billion year old temperature fluctuations (shown as color differences) that correspond to the seeds that grew to become the galaxies. The signal from the our Galaxy was subtracted using the multi-frequency data, seen below. This image shows a temperature range of ± 200 microKelvin. - Credit: NASA / WMAP Science Team

The first one lead to new gravitation theories (e.g.: the so-called MOND, MOdified Newton Dynamics theory), which anyway hardly explain both local and large scale observations at the same time.

This work is based on the latter assumption. The most commonly proposed DM candidates are axions, sterile neutrinos, and WIMPs (Weakly Interacting Massive Particles, including neutralinos). In any case, introducing such kind of particle into models means to probe new Physics beyond the Standard Model. In this frame, supersymmetric models come to aid and in this work we focus our attention on one of the most studied and discussed Supersymmetric WIMP candidate, the *neutralino*.

2.2 Supersymmetry

Supersymmetry (often abbreviated SUSY) is a symmetry that relates elementary Standard Model particles of one spin to other particles that differ by half a unit of spin (known as superpartners). So far, there is no direct evidence for the existence of supersymmetry. That means that it is a *broken* symmetry and its energy scale must be

Normal particles/fields		Supersymmetric partners			
		Interaction eigenstates		Mass eigenstates	
Symbol	Name	Symbol	Name	Symbol	Name
$q = d, c, b, u, s, t$	quark	$\tilde{q}_L$, $\tilde{q}_R$	squark	$\tilde{q}_1$, $\tilde{q}_2$	squark
$l = e, \mu, \tau$	lepton	$\tilde{l}_L$, $\tilde{l}_R$	slepton	$\tilde{l}_1$, $\tilde{l}_2$	slepton
$\nu = \nu_e, \nu_\mu, \nu_\tau$	neutrino	$\tilde{\nu}$	sneutrino	$\tilde{\nu}$	sneutrino
g	gluon	$\tilde{g}$	gluino	$\tilde{g}$	gluino
$W^\pm$	W-boson	$\tilde{W}^\pm$	wino	$\tilde{\chi}^\pm_{1,2}$	chargino
H^-	Higgs boson	$\tilde{H}^-_1$	higgsino		
H^+	Higgs boson	$\tilde{H}^+_2$	higgsino		
B	B-field	$\tilde{B}$	bino	$\tilde{\chi}^0_{1,2,3,4}$	neutralino
W^3	W^3-field	$\tilde{W}^3$	wino		
H^0_1	Higgs boson	$\tilde{H}^0_1$	higgsino		
H^0_2	Higgs boson	$\tilde{H}^0_2$	higgsino		
H^0_3	Higgs boson				

Figure 2.5: susytable - Standard Model particles and their supersymmetric partners in MSSM.

higher than the energy range so far investigated by accelerators. There are strong theoretical motivations (and hopes) that Supersymmetry lays close to the electroweak scale (GeV÷TeV):

- it provides a solution to the hierarchy problem (i.e.: how to naturally explain the gap between the weak force scale and gravity scale);
- it provides a natural mechanism for electroweak symmetry breaking;
- it allows unification of gauge couplings of the three gauge groups at high energies;
- it naturally generates the perfect WIMP DM candidate;

The simplest known method to introduce new supersymmetric partners into the SM is the so-called Minimal Supersymmetric extension of the Standard Model (MSSM).

The MSSM imposes R-parity to explain the stability of the proton. This quantity is defined as:

$$R \equiv (-1)^{3B+L+2S} \tag{2.4}$$

from the quantum numbers B (baryon number), L (lepton numer) and S (spin), so that R = +1 for SM particles and R = -1 for SUSY particles.

The conservation of R-parity implies that in SM particles interactions SuSy particles can be produced only in pairs and also that SuSy particles can only generate final states with odd number of SuSy particles. In this frame, it is clear the Lightest Supersymmetric Particle (LSP) is stable since there will be no allowed state with negative R for the decay.

In MSSM the neutralinos are four Majorana fermions, result of the mixture of superpartners of the B, W_3 gauge bosons (bino, wino) and the neutral Higgs bosons H_1^0 and H_2^0 (higgsinos). The four neutralinos are denoted as χ_i^0 for $i = [1, 4]$ with increasing mass. In this work we will focus on the lightest one, simply *the* neutralino χ, becasuse it is the most favoured candidate as dark matter, but our analysis is actually quite model independent.

The lightest neutralino, χ , can be expressed as :

$$\chi \equiv \tilde{\chi_0^1} = n_{11}\tilde{B} + n_{12}\tilde{W}_3 + n_{13}\tilde{B} + \tilde{H_1^0} + n_{14}H_2^0 \tag{2.5}$$

where n_{ij} are the elements of the neutralino mass mixing matrix.

Although very appealing and based on elegant principles, the MSSM is still a rather complicated framework to work with, because of its many parameters.

2.3 Indirect and Direct Detection

The only information we have about DM distribution in the Universe is so far due to large-scale gravitational effects.

Neutralinos undergo weak and gravitational interactions only. They are expected to scatter off nuclei through both scalar spin-independent (SI) and axial spin-dependent (SD) interactions, the strength of each coupling determined by the MSSM model. SD cross-section is proportional to $J(J + 1)$, while SI cross-section is proportional to A^2, thus increasing with the mass of target nuclei.

Many current experiments are trying to detect supersymmetric dark matter both directly and indirectly.

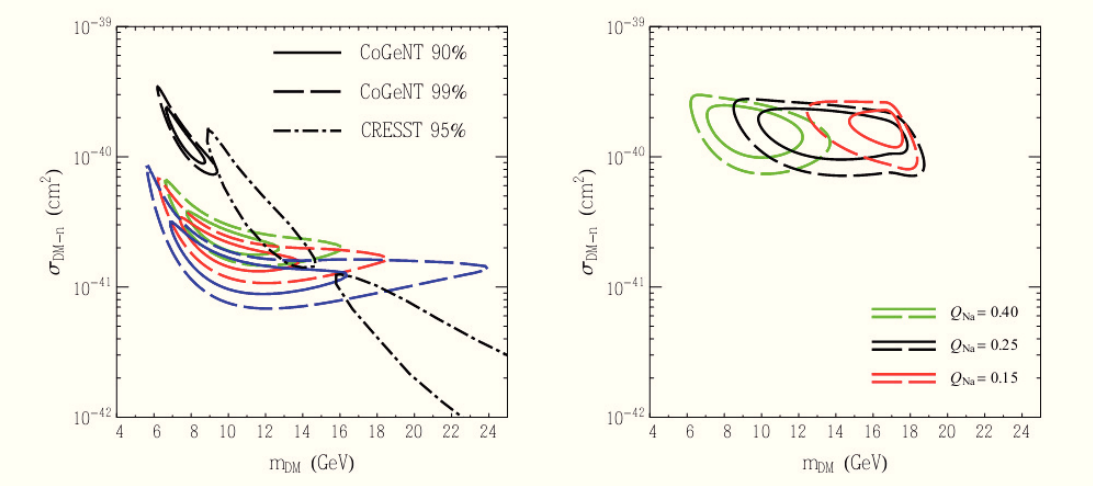

Figure 2.6: DAMA-CRESST-CoGeNT - Left - The 90% (solid) and 99% (dashed) confidence level contours for the spectrum of events observed by CoGeNT, The CRESST contours (dot-dashed) denote the 95% confidence level regions. A dark matter particle with a mass of approximately 10-20 GeV and an elastic scattering cross section with nucleons of approximately 10^{-41} cm^2 can account for the excess events reported by each of these experiments. **Right** - The 90% (solid) and 99% (dashed) confidence level contours for the spectrum of the amplitude of the annual modulation observed by DAMA/LIBRA, assuming a simple Maxwellian velocity distribution with v_0 = 220 km/s and $vesc$ = 544 km/s. Taken from (23)

2.3.1 Direct Search

The basic idea of dark matter direct search is to detect the recoil energy of nuclei scattered off by WIMPs. The main contribution to the scattering process is due to the SI interaction, since heavy nuclei are usually used. The expected WIMP scattering rates in direct searches are generally small, and the WIMP recoil-spectrum is not much different from the background at low energies. However, the annual modulation of the scattering rate can be used as a specific signature in order to disentangle a DM signal from the background.

This effect, expected to be of the order of a few percent, is induced by the rotation of the Earth around the Sun, which periodically changes the DM flux relative to the detector, and it is known to be a smoking gun signature for DM detection. Observation of such an annual modulation signal has long been claimed by the DAMA/LIBRA experiment (9), a detection that has by now reached a significance of 8.9σ, and can be interpreted in terms of the scattering of a light WIMP of mass ≈ 10 GeV off sodium nuclei.

A similar light WIMP explanation has been invoked to explain the low energy excess reported by the CoGeNT experiment in 2010 (11), as well as the more recent CRESST results (12). However, these results are at the same time excluded by a number of null searches, most notably XENON (14) and CDMS(13). Adding further to the puzzle, the CoGeNT collaboration recently reported a modulating signal in the energy range $0.5 \div 3.0$ KeV at 2.8σ, with a modulation amplitude of $16.6 \pm 3.8\%$, a period of 347 ± 29 days, with the minimum rate falling on October rather than the predicted December (23).

2.3.2 Indirect Search

Indirect detection focuses on observing particles emitted by WIMP annihilations. One of the methods is to use satellites in search for positrons, antiprotons, antideuterium and gamma excesses (e.g.: the PAMELA experiment (15), the Fermi experiment (16)).

The antiproton flux and the positron flux have recently been measured by the PAMELA experiment in the 1-100 GeV energy range. Although there is reasonable agreement between the measured antiproton flux and the expected background, the measured positron flux is incompatible with the expected background. One proposed

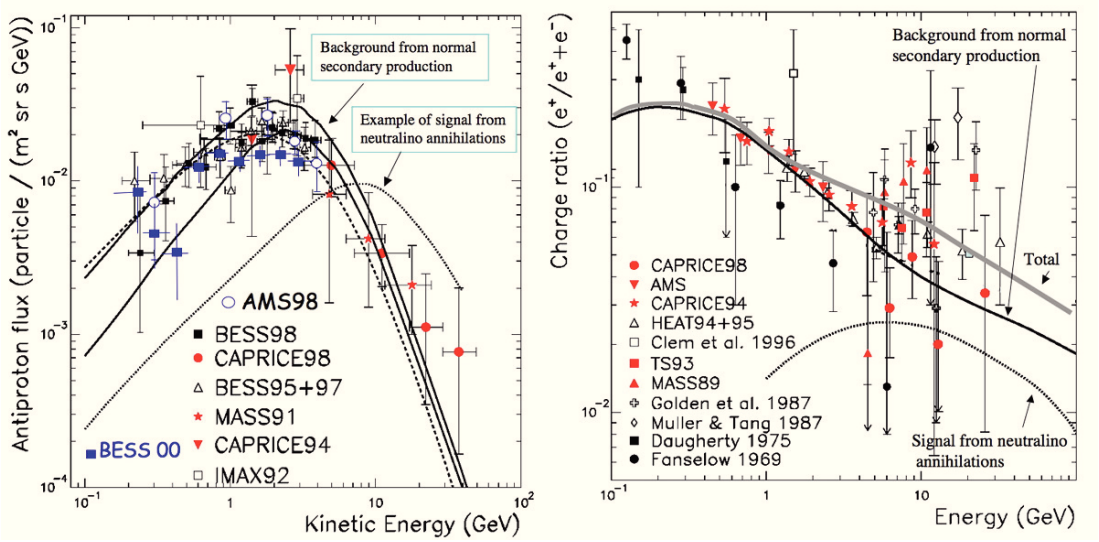

Figure 2.7: Pamela excess - WIMPs could contribuite to the positron flux by direct annihilation in e^+e^- , and to continuum positrons from the other annihilation channels. This could be seen as an excess or bump beginning at a few GeV and extending upward in energy to a point depending on the WIMP mass.

solution was that it could be an indication of DM annihilating into leptons. Anyway, the debate is still open and there are many other explanation to that. The most shared belief is that close pulsars might accelerate particles in their magnetosphere thus producing cascades.

Gamma-rays point directly to the source, making their source's identification easier than charged particle. The Fermi Telescope investigated the energy range 20 MeV ÷ 300 GeV, in search of signals coming from near objects like the Galactic Center, (19) and extragalactic , but still no excess is found. Also the HESS Collaboration (35) provided many analysis in the energy range ~100 GeV ÷ 10 TeV for extragalactic source, but no evidence of signal stricly related to DM annihilation is found.

A third type of expected signal is that of neutrinos, searched for by neutrino underwater (or underice) telescopes. Neutrinos are electrically neutral fermions that only interact through the weak interaction. Neutrinos can be produced in WIMP annihilation processes. The ideal detection channel would be the direct $\chi\chi \rightarrow \nu\bar{\nu}$ process. Since WIMPs are non-relativistic, this would result in mono-energetic neutrinos with energies equal to the WIMP mass. However, this channel is helicity-suppressed for non-relativistic WIMPs that are scalar particles or Majorana fermions. In that case,

neutrinos are mainly produced through secondary production channels, resulting in a continuous energy spectrum with a cutoff at the WIMP mass. This topic will be discussed later.

2.3.3 SuSy at LHC

Another important way to investigate SuSy DM is provided by accelerators. A typical signature is a final state of multi-jets together with significant missing transverse energy, E_T^{miss}. The main processes involve the production of sleptons and squarks which eventually decay into SM and SuSy particles up to the LSP neutralino which escapes the detector.

Both CMS (17) and ATLAS (18) at CERN LHC(Large Hadron Collider) can infer importants constraints on this topic. With $\approx$ 35 fb^{-1} (radiply approaching to 50) integrated luminosity collected in pp-collisions at a center-of-mass energy of 7 TeV, both Collaborations provided competitive constrains in the so-called constrained minimal supersymmetric extension of the Standard Model (CMSSM), or minimal supergravity (mSUGRA), framework. Some of these results and predictions will be compared to those of this work.

3

Neutrino Flux from Neutralino Annihilations in the Sun

The neutralino is a perfect CDM candidate, because it is a non-relativistic electrically neutral and stable particle produced as a thermal relic of Big Bang. The mass and cross-section of the neutralino is set by the weak force, and it will therefore freeze out from thermal equilibrium in the Universe with a relic density suitable for dark matter. In an expanding and cooling Universe's frame, neutralinos lose less energy than baryons due to the low cross-sections, and it is likely that they have accumulated in a way different to the baryon clustering. Anyway a massive source can trap inside its gravitational well those WIMPs which lose enough energy scattering off nucleons, relegating them into its inner core. Once trapped their density will increase substantially and they will start to annihilate and produce SM particles (e.g. neutrinos). We will briefly show some calculations related to the neutrino fluxes coming from neutralino annihilations into the core of the Sun, but the argument also applies at the center of the Earth.

3.1 Capture Rate, Cross-sections and Expected Fluxes

WIMPs interact very rarely but they can happen to scatter off nuclei and lose energy. When they lose enough energy interacting inside a massive object (e.g. the Sun) they can be trapped by the gravitational potential and forced to travel with elliptical orbits like comets. It's reasonable that those WIMPs will undergo subsequent scatterings, stretching their trajectories losing energy at each interaction, until they will eventeually

accumulate into the solar core. A generic species of WIMPs present in the solar system will scatter elastically and become captured in the Sun at a rate given by (54), (55):

$$C_C \simeq 3.35 \cdot 10^{20} s^{-1} \left(\frac{\rho_{local}}{0.3 GeV cm^{-3}}\right)\left(\frac{270 km/s}{\bar{v}_{local}}\right)^3 \left(\frac{\sigma_{H,SD} + \sigma_{H,SI} + 0.07\sigma_{He,SI}}{10^{-6} pb}\right)\left(\frac{100 GeV}{m_{WIMP}}\right)^2 \tag{3.1}$$

where ρ_{local} is the local dark matter density, $\bar{v}_{local}$ is the local rms velocity of halo dark matter particles and m_{WIMP} is the dark matter particle's mass. $\sigma_{H,SD}$, $\sigma_{H,SI}$ and $\sigma_{He,SI}$ are the spin-dependent (SD) and spin-independent (SI) elastic scattering cross sections of the WIMP with hydrogen and helium nuclei respectivel.

The number of neutralinos in the Sun, N, can be described by the differential equation:

$$\frac{dN}{dt} = C_C - C_A N^2 - C_E N \tag{3.2}$$

where C_C, C_A, C_E are the capture, annihilation and eveporation rates respectively. The latter can be neglected for $E \gtrsim 10 GeV$, which is below the range of interest of this work. C_C depends on the scattering cross-sections on the elements in the Sun and C_A depends on the annihilation cross-section.

The neutralino annihilation rate Γ_A is :

$$\Gamma_A = \frac{1}{2} C_A N^2 = \frac{1}{2} C_C \tanh^2(t/\tau) \tag{3.3}$$

with $\tau = (C_A C_C)^{-1/2}$. The present rate is $\Gamma_A(t = t^{\odot})$, with $t^{\odot} = 4.5 \cdot 10^9$ years. If the capture rate and annihilation cross sections are sufficiently large, equilibrium will be reached between these processes, when $(t^{\odot}/\tau) \gg 1$, annihilation and capture rate are in equilibrium ($dN/dt = 0$) and

$$\Gamma_A = \frac{1}{2} C_C \tag{3.4}$$

Thus, in equilibrium, Γ_A only depends on the capture rate C_C (i.e. the capture cross-section) and not on the annihilation cross-section.

The exact value of Γ_A (as well as C_C) varies over a huge range of values ($10^4 \div 10^{15}$) with respect to the choice of the model, to the DM particle's mass and distribution.

3.2 Fluxes

Neutralinos can annihilate generating neutrinos through different channels. Annihilations to heavy quarks, tau leptons, gauge bosons and Higgs bosons can all generate neutrinos in the subsequent decays.

The generated differential neutrino flux can be written as:

$$\frac{dN_\nu}{dE_\nu} = \frac{\Gamma_A}{4\pi d^2} \sum_f BR_f \frac{dN_f}{dE} \tag{3.5}$$

where f runs over the final states of the DM annihilations with branching ratios BR_f and d is the distance of the source from the detector, dN_f/dE is normalized to a single annihilation.

In this work we follow the approach of (5) using the publicly provided fluxes for our analysys. These fluxes, generated with PYTHIA code (6), are calculated for the main annihilation channels ($\nu\bar{\nu}$, $b\bar{b}$, $\tau\bar{\tau}$, $c\bar{c}$, light quarks, ZZ, W^+W^-, ...). They include propagation out of the source up to the Earth, including neutrino oscillations. For an exahustive review we refer to the full article.

The 3.5 provides neutrino fluxes from neutralino annihilation propagated at Earth. The actual signal at detector will depend on the sum over all channels f of all neutrino fluxes weighted with their branching ratios BR_f. Since branching ratios are strongly model-dependent, we chose for our analysis the annihilation channels with the "softest" and the "hardest" neutrino spectra as worst and best case, respectively.

For comparison with other results, we chose:

$$\chi\chi \rightarrow b\bar{b} \tag{3.6}$$

$$\chi\chi \rightarrow W^+W^- \tag{3.7}$$

as a "soft" and a "hard" channels respectively.

3.3 Neutrino fluxes from WIMP annihilations in the Sun

In this section we focus on a brief description of neutralino annihilation channels, paying attention to those channels whose signal could be of greater interest to Čerenkov neutrino telescopes ($\gtrsim$ 100 GeV). In figures 3.1, 3.3, 3.5 are shown neutrino spectra at

production (at the center of the Sun) and in figures 3.2, 3.4 and 3.6 the same spectra after taking account of propagation up to Earth and oscillation effects.

For trivial reasons, the direct channel $\chi\chi \rightarrow \nu\bar{\nu}$ would in principle produce the hardest and most energetic neutrino spectrum. At production, it would just be a monocromatic line at around m_χ. In the neutralino case, since χ is a Majorana particle, it can only decay into $f_L\bar{f_R} + \ldots$ with an annihilation amplitude which is proportional to the mass of the fermion, so the most important channels are the heavier ones (e.g.: $b\bar{b}$, $\tau\bar{\tau}$, $c\bar{c}$, $t\bar{t}$).

3.3.1 Annihilation into fermions

Light quarks (u, d, s) mostly hadronize into pions, which are stopped in the medium and do not produce neutrinos in an interesting energy range. Their contribution to the total spectra in mainly due to subsequent production of a c quark but this contribution can be safely neglected in first analysis.

Annihilation into $b\bar{b}$

The bottom quark channel always gives the softest spectrum for any neutralino mass. In fact, b quarks hadronize into B-hadrons which undergo weak interaction losing a significant amount of energy (lifetime $\sim 10^{-12}$ s) with surrounding matter, if density is high enough.

Annihilation into $t\bar{t}$

If accessible (i.e. $m_\chi \gtrsim m_t \approx 173GeV$), the top quark channel is similiar to the bottom's one, but a bit harder. This is due to the high mass of t translating into short livetime of $\sim 10^{-25}$ s, which will produce a W-boson and a b quark before losing significant amount of energy. The light quark can produce a soft neutrino spectra (see above), the W can decay into a neutrino and a charged lepton as will be shown below, thus boosting the spectrum.

Annihilation into $\tau^+\tau^-$

The τ channel will give the hardest spectrum for any m_χ amongst fermions. Tau's lifetime of about $3 \cdot 10^{-13}$ s is short enough to allow its decay before it can interact

with its surroundings, decaying into a tau-neutrino and a lepton-neutrino pair with $BR \sim 17.5\%$ each, providing quite hard neutrino spectra.

3.3.2 Annihilation into Gauge bosons $W^{\pm}$ and Z_0

Neutrinos are also produced by the annihilation into Gauge bosons W^+W^-, ZZ, which happen to produce very hard spectra because the prompt neutrino emission by $W_l \rightarrow \nu_l \bar{l}$ and $Z \rightarrow \nu_l \bar{\nu}_l$ significantly boosts the final flux. The produced spectra are very similiar, but the lepton produced by W will eventually produce further neutrinos with softer spectra.

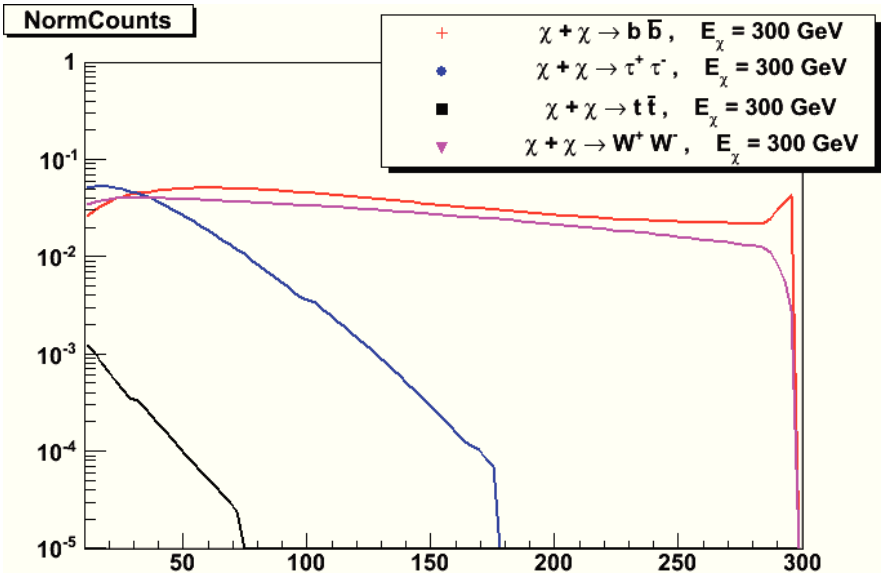

Figure 3.1: 300 GeV Spectra at production. - Energy spectra of produced neutrino fluxes at production coming from 300 GeV DM particle annihilating into the Sun, for different channels.

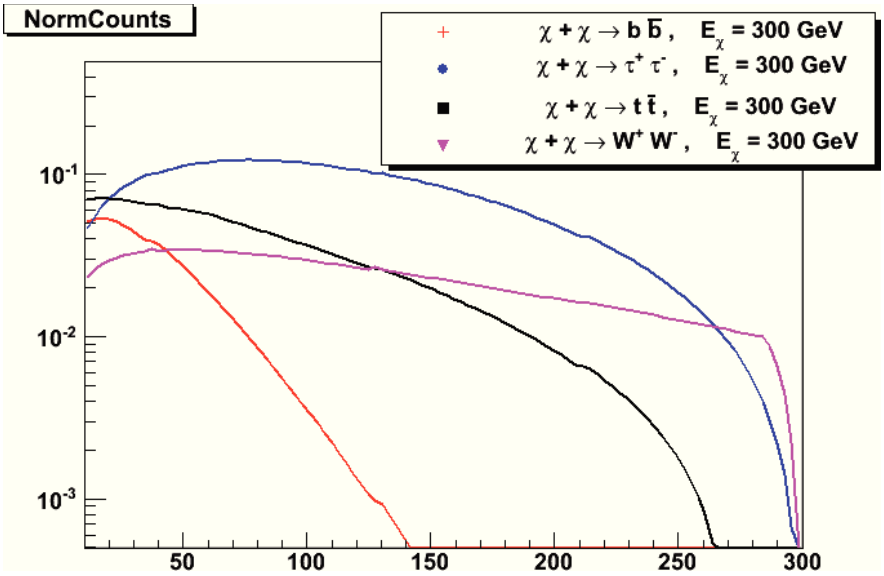

Figure 3.2: 300 GeV Spectra at detector. - Energy spectra of propagated neutrino fluxes at detector coming from 300 GeV DM particle annihilating into the Sun, for different channels.

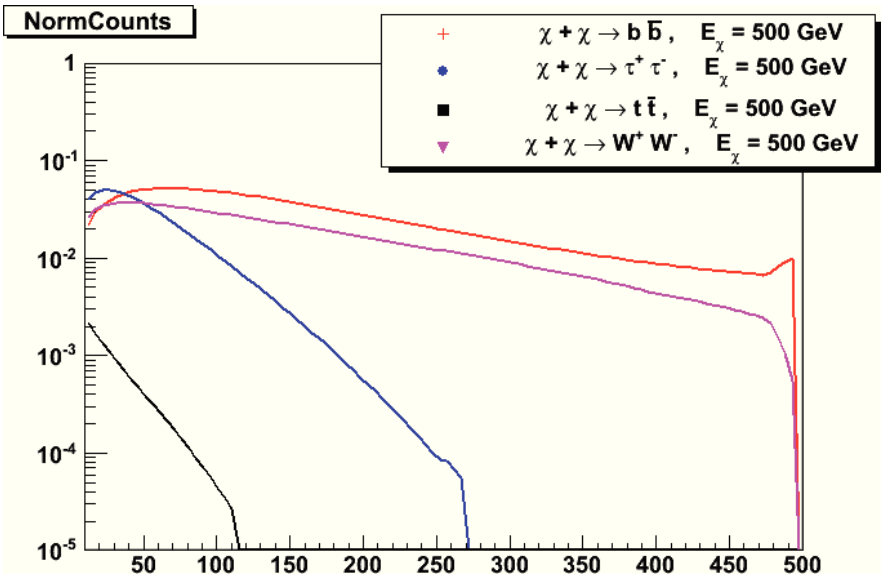

Figure 3.3: 500 GeV Spectra at production. - Energy spectra of produced neutrino fluxes at production coming from 500 GeV DM particle annihilating into the Sun, for different channels.

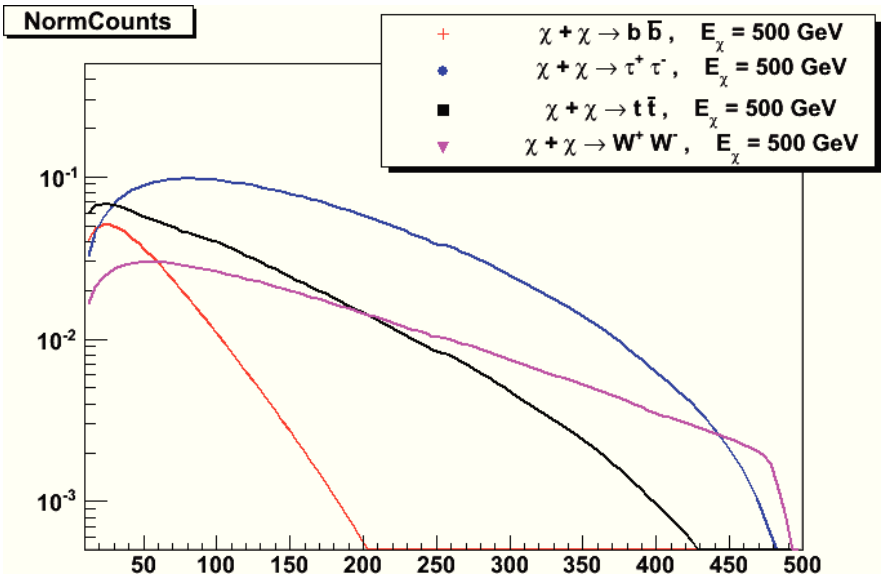

Figure 3.4: 500 GeV Spectra at detector. - Energy spectra of propagated neutrino fluxes at detector coming from 500 GeV DM particle annihilating into the Sun, for different channels.

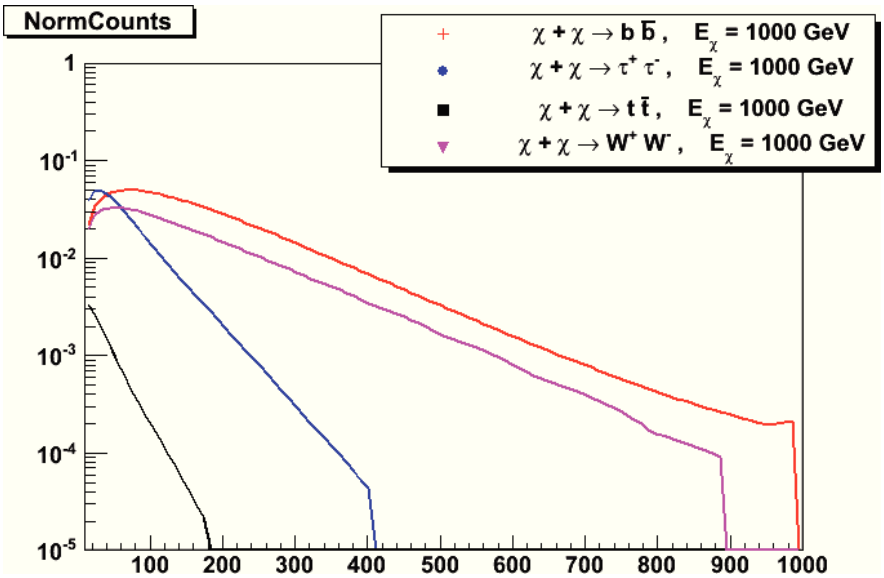

Figure 3.5: 1 TeV Spectra at production. - Energy spectra of produced neutrino fluxes at production coming from 1 TeV DM particle annihilating into the Sun, for different channels.

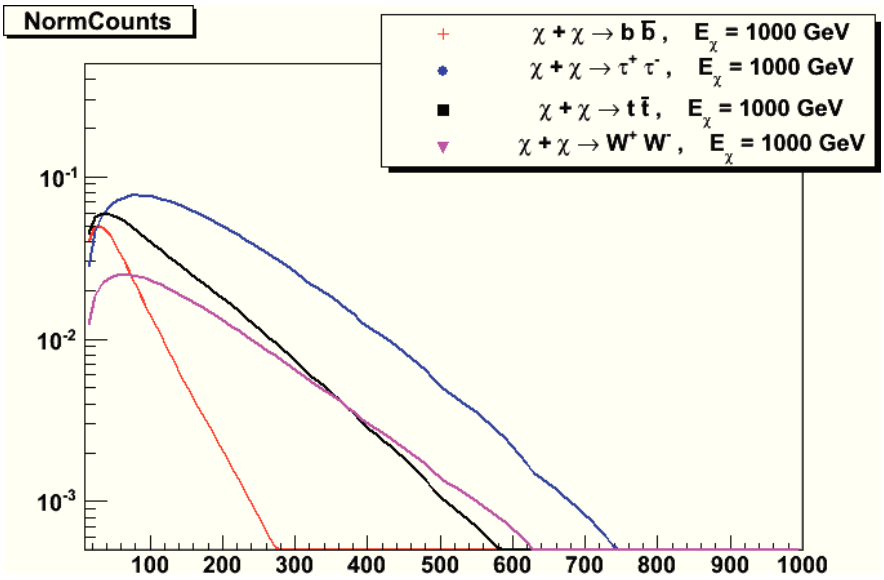

Figure 3.6: 1 TeV Spectra at detector. - Energy spectra of propagated neutrino fluxes at detector coming from 1 TeV DM particle annihilating into the Sun, for different channels.

4

Neutrino detection

The Universe is a huge source of information. Galactic and extra-galactic astrophysical objects fill the *space* with radiation which carries precious information about close and distant Universe.

Gamma and proton astronomy are providing important informations on astrophysical sources and precious insights on the comprehension of the Universe. Even though in rapid development, these kinds of astronomy has some insurmountable limitations. Very far sources are very hard to study by means of Very High Energy photons, because of their absorption due to the interstellar medium. TeV (or more energetic) photons are likely to interact with the CMB (microwave, infrared,...) by pair production $e^- e^+$ and photopion production at higher energies . On other hand, proton (and heavy nuclei) astronomy faces the problem of the deflection of the proton by the Galactic and inter-galactic Magnetic Fields, thus making the tracking to the original source of the particle hard to fulfill.

The importance of neutrino astronomy lays in the double-edged behaviour of its probe. Neutrino's most remarkable feature is its very low probability of interaction with matter. At the beginning, it represented a huge obstacle to its discovery and study, but now it is also a brilliant quality. On one hand, since neutrinos interact only *weakly* with matter they can easly reach the Observer from sources billions of lightyears away carrying unaltered informations. On the other hand, for the very same reason they are very difficult to detect. On the behalf of this 50-years-old idea, the first projects on underwater neutrino telescopes were born. Even though they still hold many secrets,

today we know much about neutrinos and thanks to this knowledge the neutrino acquires a new role as astrophysical probe.

4.1 Neutrino Interaction

The neutrino can interact with matter by the exchange of a charged $W^{\pm}$ or neutral Z gauge boson with a quark in the nucleon N (Fig.4.1).

The first case, called Charged-Current (CC) interaction, can be written as:

$$\nu_l + N \rightarrow l + X \tag{4.1}$$

where ν_l can be neutrino (or anti-neutrino), X is a hadronic shower produced together with thethe lepton (or anti-lepton) l with the same flavour as the interacting neutrino.

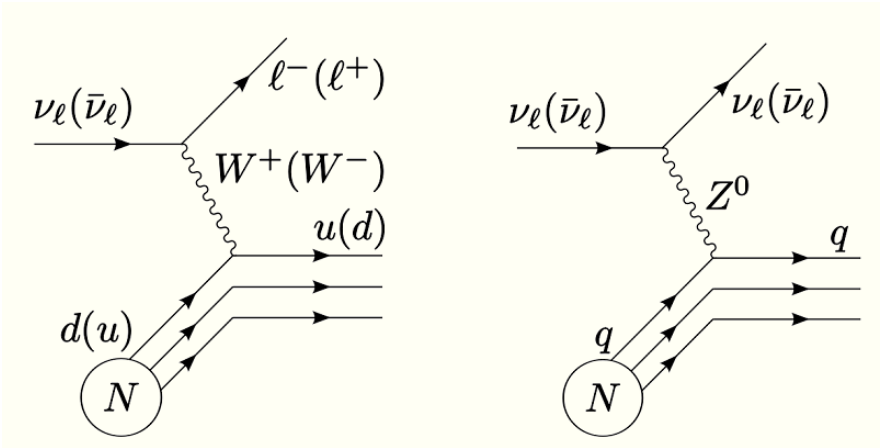

Figure 4.1: Neutrino Interactions - Left: Charged Current interaction - Right: Neutral Current Interaction

The other one is the so-called Neutral-Current (NC) interaction:

$$\nu_l + N \rightarrow \nu_l + X \tag{4.2}$$

describing a neutrino scattering off a nucleon N producing a hadronic shower X.

In the case of a ν_{mu}-nucleon CC interaction, the angle between the neutrino and the muon is described by:

$$\langle \theta_{\nu-\mu} \rangle \propto \frac{1}{\sqrt{E_{nu}}} \tag{4.3}$$

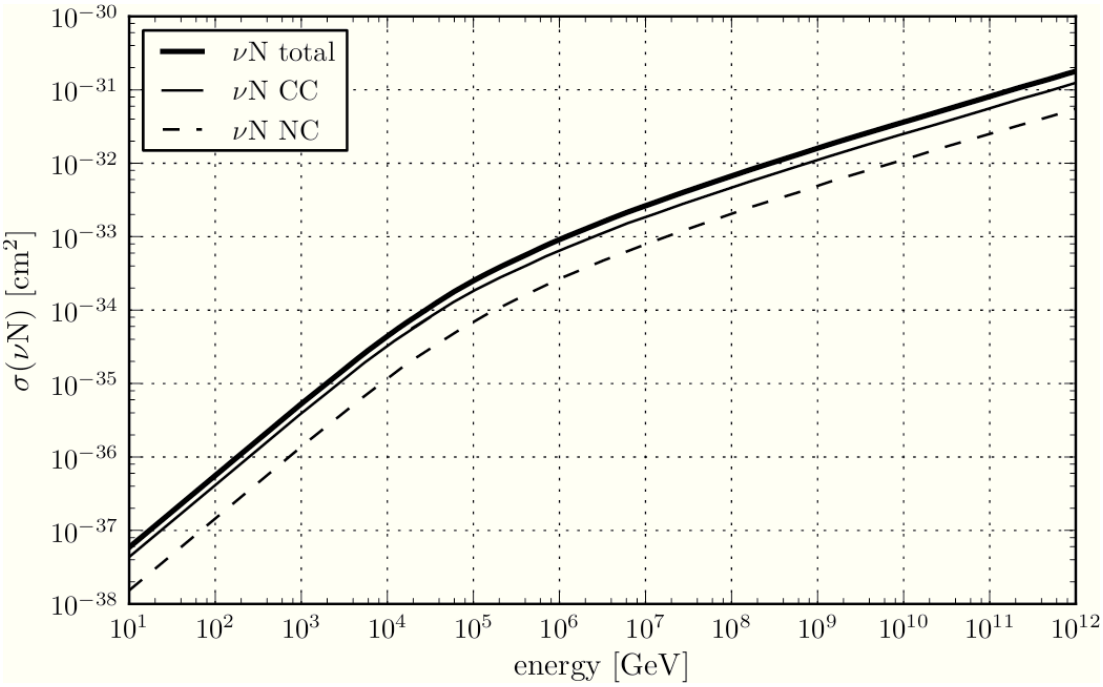

Figure 4.2: Neutrino CS - Neutrino-nucleon cross-sections for CC and NC interactions

with E_{nu} given in TeV. It is about 1.5^o at TeV and at higher energies this angle becomes small, thus the muon and the neutrino are almost collinear. Tracking the muon gives a very good information about the neutrino's direction as well.

4.2 Neutrino oscillation

There are three known types (flavors) of neutrinos: electron neutrino, muon neutrino and tau neutrino, named after their partner leptons in the Standard Model.

Their flavour eigenstates $|\nu_\alpha\rangle = (\nu_e, \nu_\mu, \nu_\tau)$ differ from their mass eigenstates $|\nu_i\rangle = (\nu_1, \nu_2, \nu_3)$.

The flavour and mass eigenstates are note the same. They are linear superpositions of one another, and can be related by the leptonic mixing matrix $U_{\alpha i}$ (the Pontecorvo-MakiNakagawaSakata matrix)

$$|\nu_\alpha\rangle = \sum_{i=1,2,3} U^*_{\alpha i} |\nu_i\rangle \quad \Longleftrightarrow \quad |\nu_i\rangle = \sum_{\alpha=e,\mu,\tau} U_{\alpha i} |\nu_\alpha\rangle \tag{4.4}$$

As a neutrino propagates, the misalignment of neutrino flavours and mass eigenstates causes neutrinos to periodically *change flavour*, giving rise to the so-called *oscillation* of the neutrinos.

The exact mass scale of neutrinos is still unknown, but different measurements constrain it at $\lesssim$ eV scale.

4.3 Neutrino-induced muons

Muons can cover a considerable distance before losing all their energy and dacaying. Muon energy loss in water is dominated by four processes: ionization and excitation, pair production, bremsstrahlung and photo-nuclear interaction. For $E_{mu} \lesssim 1TeV$ (which is the energy range of interest for this work), muons lose their energy mainly by ionization and excitation, due to the elastic scattering on atomic electrons in the medium. The muon range in water depends on the muon energy loss rate which is strongly dependent on the particle's energy.

Muons also lost a small amount of energy by polarizing the atomic electric field in its srurroundings. When the muon has passed the field is de-polarized by emission of photons. This is called Čerenkov Effect.

4.4 The Čerenkov Effect

When a charged particles crosses a medium while moving at speed greater than the speed of light in medium, it emtis a characteristic radiation along its path. That is the result of the coherent de-polarization of the atoms surrounding the particle's path. Čerenkov emission is indeed emitted within a cone with angle ϑ_c, which depends on the particle velocity β and on the refractive index n of the crossed medium (Fig. 4.3), by the relation:

$$\cos \vartheta_c = \frac{1}{\beta < n >} \tag{4.5}$$

in case of sea water ($n \approx 1.4$) and high energy muons ($\beta \approx 1$) we have $\vartheta_c \approx 42°$.

The directionality of Čerenkov radiation strictly relates the produced photon with the emitting particle's position at given time, granting the possibility to reconstruct the particle's trajectory inside the medium.

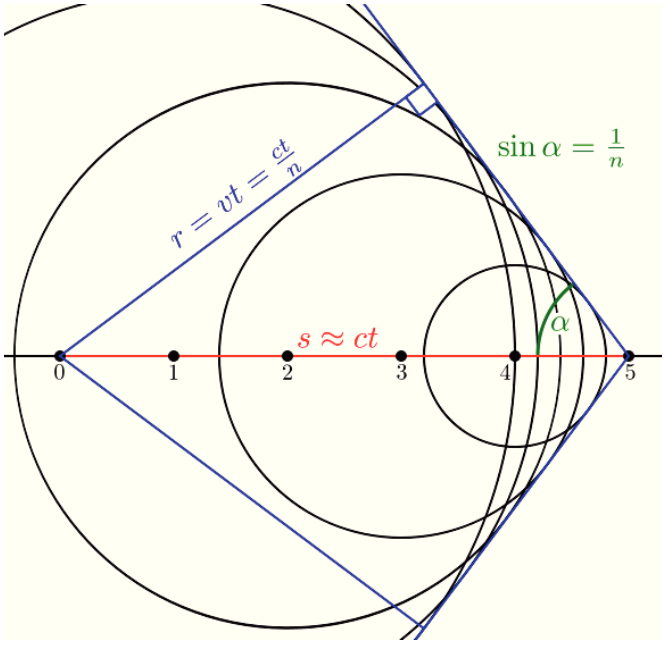

Figure 4.3: Čerenkov Radiation - Čerenkov radiation from a charged particle nearly at the speed of light moving in a medium with index of refraction n.

4.5 Light propagation

Propagation of light inside a medium is affected by absorption and scattering, and it can be described by the absorption lenght λ_a and scattering lenght λ_s, i.e. the average distances at which the intensity of the photon field is reduced by a factor $1/e$ due to absorption processes and scattering procecesses with the medium respectively.

For Mediterranean Sea (Capo Passero, the candidate site of the NEMO Collaboration (27), (36)) at $\lambda = 473$ (375)nm absorption lenght is 60 ± 10 (26 ± 3) m and scattering lenght is 270± 30 (120 ± 10)m.

For ICECUBE (ice) abosrption lenght is 110m, scattering lenght is 20m at $\lambda = 400$nm.

Thus, light is less absorbed in ice rather than in water. On other hand, in ice it is more affected by scattering processes than in sea water. As a result, the light path signature in ice will generally be longer but more broadened at the same time, than in sea water.

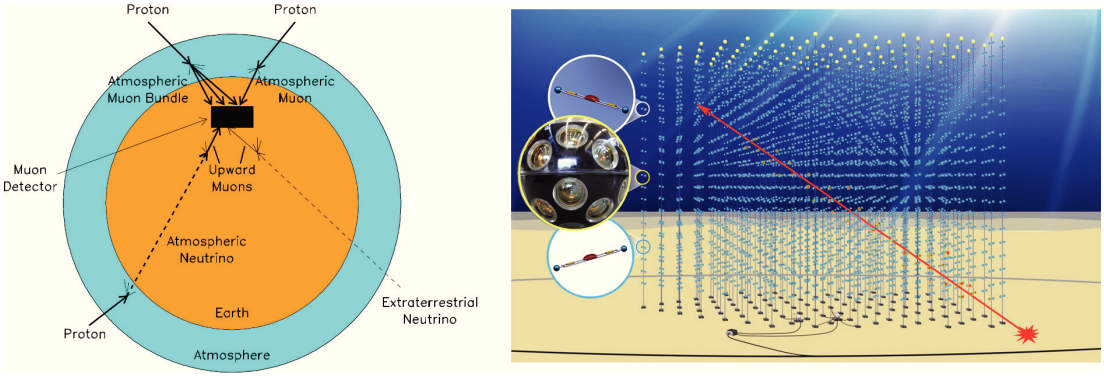

Figure 4.4: Underwater ν telescopes - Detection principles and artistic impression of a neutrino underwater Čerenkov detector.

4.6 Detection Principles

The design and the construction of high energy astrophysical neutrino detectors is a very exciting challenge for Astroparticle Physics. Neutrino's very low cross-section 4.2 forces to use a detector with large instrumented area, with a volume of several km^3 to grant sufficient statistics in a time compatible with the detector lifetime ($\sim$ 10 years).

The tecnique used for high energy netrino detection is based on some concepts:

- neutirnos undergo Charged Current (CC) interaction by eq ref; Each lepton produces a characteristic signature in an underwater(underice) neutrino telescope, also depending on its energy. The "golden channel" is the one producing muons, since muons can travel for thousands of (water equivalent) meters before losing all of their energy. Electrons will rapidly lose energy through bremsstrahlung and pair production, resulting in an electromagnetic shower. Tau has even larger mass than the muon, but it also has a much shorter lifetime ($\approx 10^{-13}$ s). Hence it travels for smaller distances than a muon before it decays, eventually producing a muon as well.

- neutrinos interact in the detector's proximity and the produced muons propagate through a transparent medium (like water or ice) emitting Čerenkov radiation, which is detected by a conveniently positioned optical sensors array;

- the directionality of the emitted radiation allows the muon track reconstrucion by means of an array of optical modules. The arrival times of the Čerenkov light at

the sensors, combined with their known spatial position, are used to reconstruct the trajectory of the particle.

- the angular resolution depends on the $\nu - \mu$ intrinsic angle and on the detector angular resolution (since at very high energies muons carry a large fraction of the neutrinos energy they have a direction that is almost identical to that of the neutrino)

There are two different kinds of background related to high-energy particles: atmospheric muons and atmospheric neutrinos. Both are due to the interaction of primary cosmic rays in the atmosphere.

The need of large instrumented volumes and the presence of huge background due to the atmospheric muons lead to use the depths of the sea (or ice) both as detecting medium (and propagator) and as a (partial) shield against CR background.

The atmospheric muon flux at sea surface exceeds that of neutrino-induced muons in the detector by about several orders of magnitude. These muons, however, are attenuated below sea surface as a function of depth and zenith angle. Their flux falls to zero near and below the horizon where they are stopped by the water and Earth shielding. For this reason astrophysical neutrino signals are mainly searched for among muons from the downward hemisphere.

4.7 High Energy Neutrino Telescopes

At the end of last century, on the behalf of these concepts the first underwater neutrino telescopes were built. BAIKAL (from the homonymous Siberian lake for the detector site) (26) and AMANDA (Antarctic Muon And Neutrino Detector Array, at the South Pole) (30), were the first high energy neutrino detectors built to provide the first limits to neutrino fluxes from astrophysical sources.

In recent times "*second generation*" Neutrino Telescopes R&D were built, with better performance and km^3 scale.

IceCube

IceCube (31), built as an AMANDA upgrade at South Pole, is the first km^3 neutrino telescope and it's taking data since more than 1 year (date of completion: December

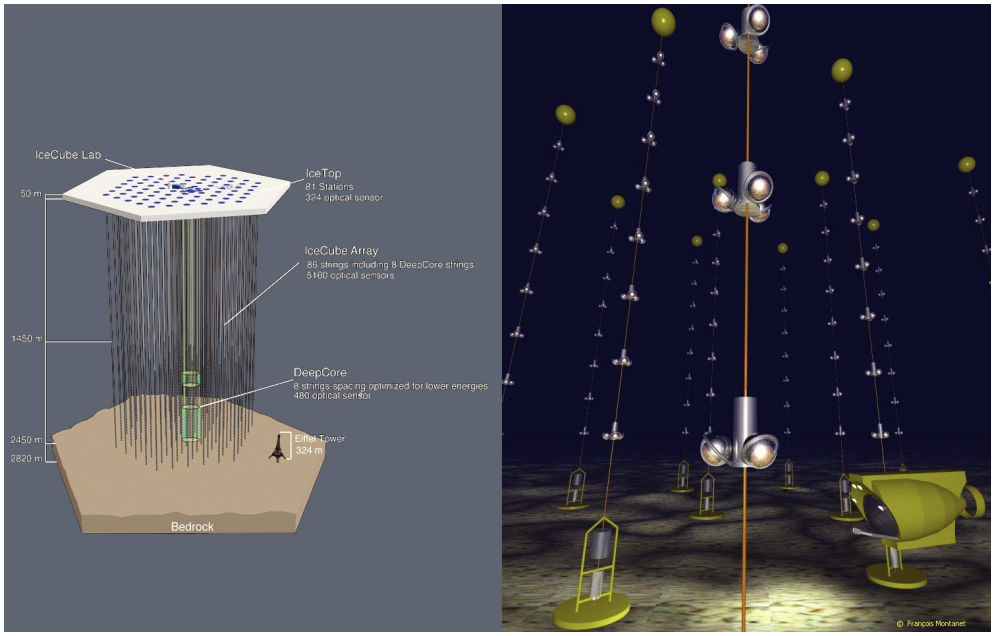

Figure 4.5: IceCube & **Antares** - Left: Artistic view of IceCube Detector at South Pole - Right: Artistic view of Antares Detector in the Mediterranean Sea

2010). It's made of 80 lines, each line hosting 60 Digital Optics Modules (DOMs) in downward looking configuration and buried in deep ice at about 2000m, an air-shower detector (IceTop) for anti-coincidence and 8 densely instrumented strings (Deep Core) for lower energy (≈ 10 GeV) neutrino Physics involving neutrino oscillations, neutrinos from Supernovae and Dark Matter search. In ice there is almost no optical background noise from either ^{40}K or bioluminescence. The antarctic ice has a much higher absorption length than water, but its scattering length is relatively short. Furthermore, the impurities trapped inside the ice are stratified according to their formation epoch and present lots of anysotropies which are hard to deal with.

ANTARES

The ANTARES (28) detector is the first completed deep-sea neutrino telescope. It is located in the Mediterranean Sea, 40 km off the French Coast at 2÷2.5 km depths. It consists of 12 strings, each with 75 (down-ward looking) optical modules distributed in triplets on 25 floors per string for a total number of 885 OMs.

It is currently taking data at full strenght since May 2008 and the ANTARES COLLABORATION is dealing with preliminary analysis.

ANTARES (28), NEMO (NEutrino Mediterranean Observatory)(27) and NESTOR(29) are European projects aiming at the construction of a km^3 neutrino telescope in the Mediterranean Sea. They are joining forces into KM3NeT project (32) in order to build the first km^3-scale neutrino telescope in the North hemisphere. KM3NeT is described in the next section.

4.8 KM3NeT

KM3NeT is a deep-sea multidisciplinary observatory in the Mediterranean Sea that will provide innovative science opportunities spanning Astroparticle Physics and Earth and Sea Science.

There are strong motivations in favour of a km3 neutrino telescope located in the Northern Hemisphere. Mainly because most of Galactic Sources lies on this Hemisphere and tagging along with IceCube we would be able to see the full sky and form a global neutrino observatory.

The Mediterranean Sea is the perfect candidate both for tecnical and pratical issues. These European Collaborations are joining forces to push forward the construction of this detector, merging into KM3NeT Consortium.

Three projects were undertaken in the Mediterranean Sea as forerunners of KM3NeT. These were the French based ANTARES, the Italian based NEMO and the Greek based NESTOR projects. The sites have shown to be valid candidate sites for hosting the KM3NeT infrastructure. Their locations are shown in Figure 4.6.

A "Technical Design Report" (TDR) has been written, describing the project in details and now the Design Study (DS) phase is about to conclude and the Preparatory Phase (PP) to begin. The outcomes of this campaigns are the guide lines for the future km^3 Mediterranean detector. Since the final design of the project is still not completely defined, in this work some of the possible detector's layouts are studied with specific focus on DM detection.

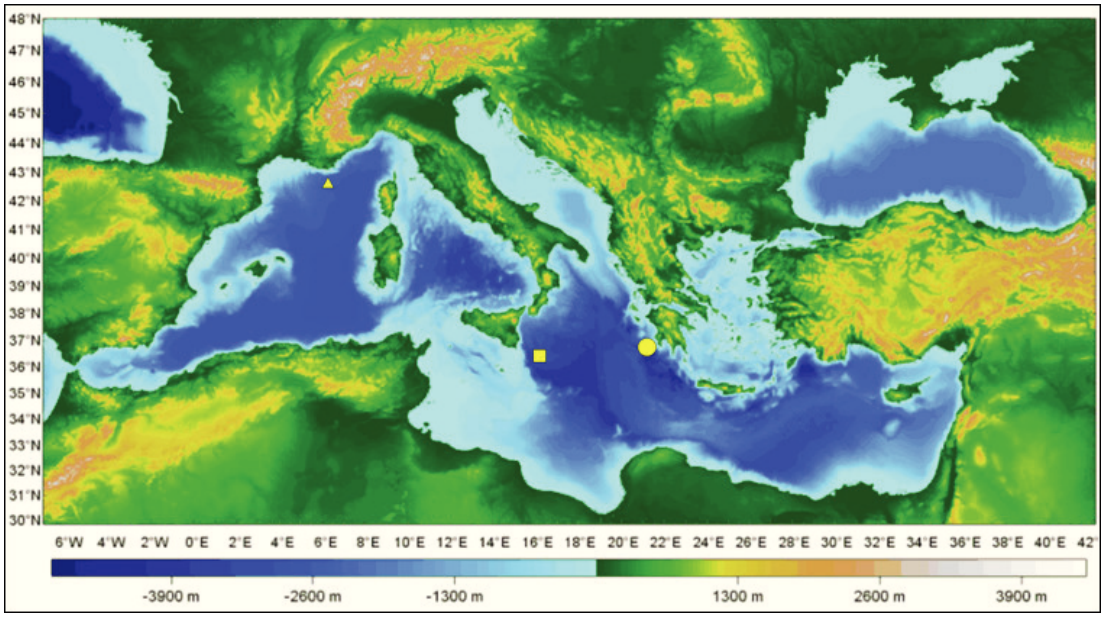

Figure 4.6: KM3NeT sites - The figure shows the three candidate sites for the future KM3NeT telescope.

4.8.1 Layout

It is trivial that the relative position of optical modules (OMs) inside the detector frame is a crucial issue.

Simulations indicate that horizontal distances of a few meters in local optical module groups greatly increase the reconstruction quality and thus the sensitivity. This topic opens a wide window of choices and compromises, the discussion of which goes beyond the scope of this work. A brief description to the reference TDR detector's layout and some newborn alternative configurations will be showed.

The TDR document follows two distinct approaches. In one approach ($large-PMT$) the detection units (DUs) are placed at large distances. The optical modules are distributed in clusters (*storeys*) along the vertical extent of the detection unit. To maximize the number of independent measurements, the optical modules at each storey are separated by several metres horizontally. The other configuration is oriented towards a denser distrubution of PMTs on strings. In this approach the clustering on the storey is achieved with small PMTs (~3") within a single optical module ($multi-PMT$).

In this work we follow the *tower* approach and in last Chapter we evaluate the

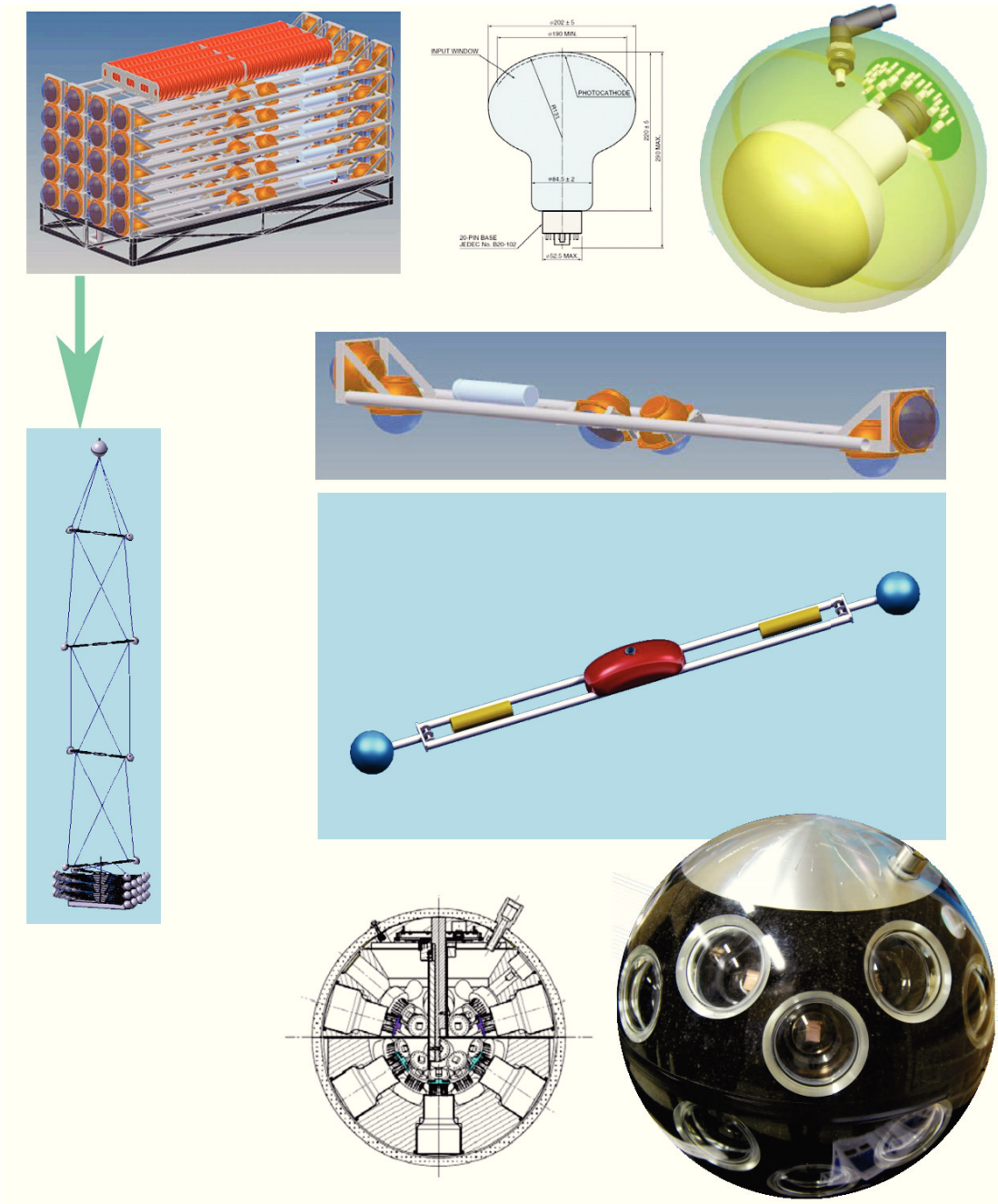

Figure 4.7: DU and PMTs - The design of a KM3NeT detection unit. The KM3NeT detection unit consists of 20 storeys with a KM3NeT-DOM at either end. The distance between storeys is 40 m. The lowest storey is located 100 m above the seabed. The schemes and images of both large-PMT and multi-PMT optical modules are shown.

performances of specific configurations to DM detection and to a more general extent. A brief description of detector layouts used for Monte Carlo simulation is given here and in Figure 4.8. A summary will be given in last Chapter.

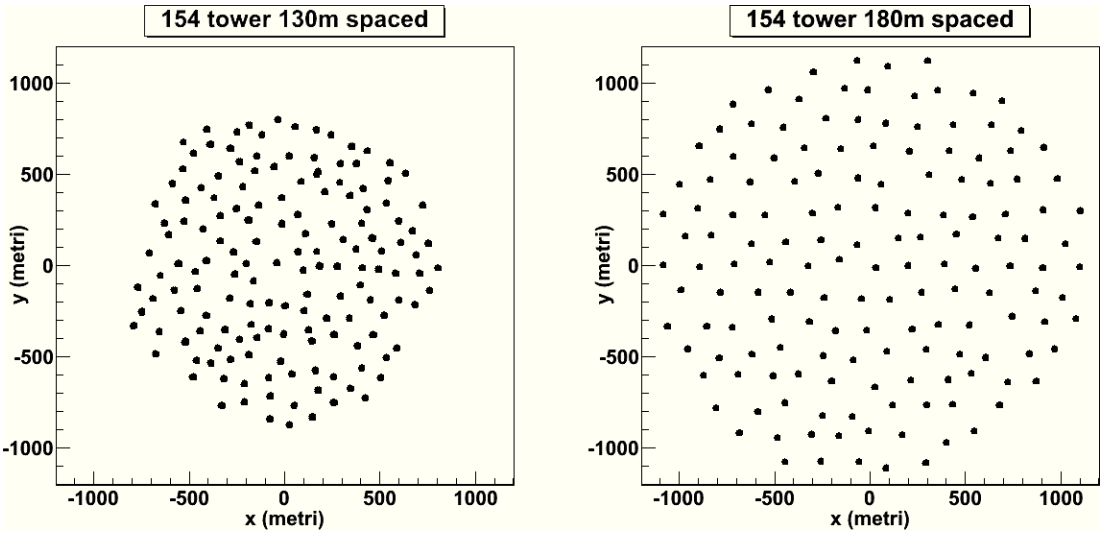

Figure 4.8: KM3NeT Layouts - The position of the Detection Units for 130m and 180m spacing

Nuone Layout

The *large – PMT* configuration (tag: *nuone*180) described in the TDR is based on NEMO Collaboration's idea. The detection unit is made of a *tower*, with 20 *bars* (storeys) hosting three pairs of PMTs with 8" diameter. Bars are 6 meters long and are spaced vertically at 40m intervals. The 8" PMTs are tubes with $\approx 1300\ cm^2$ "Super Bialkali" photocathode giving improved peak quantum efficiency of about 30% in the wavelenght range of interest (≈400nm). They are placed in pairs at the edges and at center of the bar, in a downlooking configuration, as shown in figure 4.7. The 154 towers are spaced horizontally at 180 meters, for a total of 18480 PMTs placed in an instrumented volume of roghly 3 km^3.

mPMT Layout

The *mPMT* configurations we will refer to in this work are based on TDR document's data as well. The *multi – PMT* OM consists of 31 photomultipliers of 3" diameter, with

a total photocathode surface 1260 cm^2. Their quantum efficiency is $\gtrsim$ 32% at 404nm and $\gtrsim$ 20% at470nm.

We will use 2 different *mpmt* configurations for our analysis, with the aim of evaluating each performance to *low* energy DM signals. The detection unit is a *tower* with 40m vertically spaced storeys, each one hosting a pair of $multi - PMT$ OM at its edges, 20 storyes each tower. The bar lenght is set to 6m for the first and to 10m for the othe, the spacing between towers is set respectively to 180m (tag: $ref180$) and 130m (tag: $ref130$). Therfore the instrumented volumes are different and depend on the spacing between the towers.

The final detector will consist of rougly 300 DUs. So our layouts refers to $half$ detector, since it is not excluded to have 2 detectors at different sites forming one unique array for a total of $\sim$ 300 DUs.

Altough KM3NeT primary scientific goal is the detection of high energy neutrinos from Galactic and Extragalactic particle accelerators (Supernova Remnants, Active Galactic Nuclei, ...) whose spectra are expected to lie nearly at TeV energy scales, the detector can show itself to be very competitive also at the (lower) energies of interest for dark matter searches.

4.9 Effective Area and Angular Resolution

In order to estimate the performance of a neutrino telescope two quantities are usually involved:

- Effective Area
- Angular Resolution

The effective area of a neutrino telescope is defined as:

$$A^{\nu}{}_{eff}(E_\nu, \theta_\nu) = V_{eff}(E_\nu, \theta_\nu) \times \rho N_A \times \sigma(E_\nu) \times P_{earth}(E_\nu, \theta_\nu) \tag{4.6}$$

with V_{eff} being the Effective Volume, that is the number of detected events over the generated ones, times a generation volume V_{gen}, generously encompassing the instrumented volume:

$$V_{eff}(E_\nu, \theta_\nu) = \frac{N_{det}(E_\nu, \theta_\nu)}{N_{gen}(E_\nu, \theta_\nu)} V_{gen} \tag{4.7}$$

ρN_A is the number of nucleons per unit volume (ρ is the effective matter density in mol per volume and N_A the Avogadro number), $\sigma(E_{nu})$ is the neutrino cross section in the reaction channel considered, and P_{earth} is the neutrino transmission probability through the Earth.

The angular resolution of a neutrino telescope is a quantity which relates to the muon track reconstruction accuracy. It's the error on the reconstruction between the simulated track and the reconstructed one (the angular distance $\Delta\Omega$ between the two directions).

The angular resolution of a neutrino telescope is usually defined as the Median (50^{th} percentil) of the $\Delta\Omega$ distribution, rather of the Mean Value.

Using the simulation tools described in Section 5 (page 43), one can evaluate effective area and angular resolution of the KM3NeT detector for high energy neutrinos.

For three different detector geometry, a power-law spectrum with -2 spectral index (ε_ν^{-2}) has been generated between 10 GeV and 100 PeV with isotropic flux over the whole solid angle.

4.10 Atmospheric Background

When looking for astrophysical neutrinos, there are two main sources of background which mimic their signals. They are both produced by the interaction of cosmic rays with our atmosphere, through the production of hadrons (e.g. pions and kaons) which will eventually decay into neutrinos and muons.

The atmospheric neutrinos produce a nearly-isotropic flux which follows the slope of the primary cosmic radiation spectrum. Their spectrum can be described by a power law with ≈-2.7 spectral index in most of the energy range, but at energies above 1 PeV the *prompt* neutrino emission significantly flattens the spectrum. Their signals are very hard (or nearly impossible) to be disentagled from an actual astrophysical neutrino source and thus they represent a source of unavoidable background to the detection, their event rate also surpassing the rate of astrophysical source events by several orders of magnitudes in a km^3 underwater Čerenkov detector.

The spectrum of atmospheric muons follow that of the primary cosmic radiation up to ≃ 100 GeV, where the (pion and kaon) interaction lenghts are smaller than the decay lenghst and in this region they will likely decay before interacting. The spectrum can be described as a power law with ≈-2.7 spectral index. At higher energy the interactions dominate over decay and the spectrum steepens to a spectral index of ≈ -3.7.

Muons can travel in atmosphere and in water for several kilometers but they will be stopped crossing the Earth in ≈km of *rock*, so that atmospheric muons flux is a down-going flux which extends to roughly 2π solid angle and thus directionality strongly helps in increasing the signal-to-noise ratio in a $down - looking$ detector. Despite to that, their rate at a km^3 underwater Čerenkov telescope still overcomes by 8-9 orders of magnitude the expected rate coming from any astrophysical source.

4.11 Sensitivity

When relating to a specific flux or signal the most important quantity is its Sensitivity, that is the instrument ability to detect a signal above the background, the minimum signal detectable above the background.

For neutrino telescopes, the Feldman&Cousins approach (41) is commonly used and the detector sensitivity (spectrum) can be evaluated as:

$$\left(\frac{d\varphi_\nu}{d\varepsilon_\nu}\right)_{90} = \frac{< \mu_{90}(b) >}{n_s}\left(\frac{d\phi_\nu}{d\varepsilon_\nu}\right)_{simul} \tag{4.8}$$

where $< \mu_{90}(b) >$ is the 90% Confidence Level detector sensitivity in counts using Feldman&Cousins statistics for an expected background b of atmospheric muons and neutrinos (and anti-neutrinos). n_s is amount of source events detected with respect to the simulated spectrum $(d\varphi_\nu/d\varepsilon_\nu)_{simul}$.

This quantity is of great importance because it is the actual measure of the telescope's capability to detect neutrino fluxes from astrophysical sources. The optimization of the detector with respect to a certain source is strictly linked to minimization of its sensitivity to the chosen expected flux.

5

Simulation tools

Numerical Monte Carlo simulations are needed in order to estimate the detector's performance and optimize its layout when going to compromises with financial issues. Simulation tools developed by ANTARES Collaboration and adapted for KM3NeT have been used in this work. Some modifications have been made in order to improve their use for the aim of this work.

Simulation tools

The simulation chain used in this work is made of several codes (Figure 5.1), each one with specific tasks:

GENDET - generation of the detector geometry

GENHEN - generation of muon flux and propagation to the the detector (signal and atmpospheric neutrinos)

MUPAGE - generation of muon flux at the detector (atmospheric muons background)

KM3 - muon propagation through the detector and generation of the hit due to Čerenkov photon

GEASIM - GEANT-based full simulation of propagation of secondary particles (all but muons) generated at the vertex of interaction and generation of hits due to Čerenkov photons

MODK40 - generation of white noise hits due to ^{40}K uncorrelated background on front-end electronics

RECO - reconstruction of the muon track's directions inside the detector

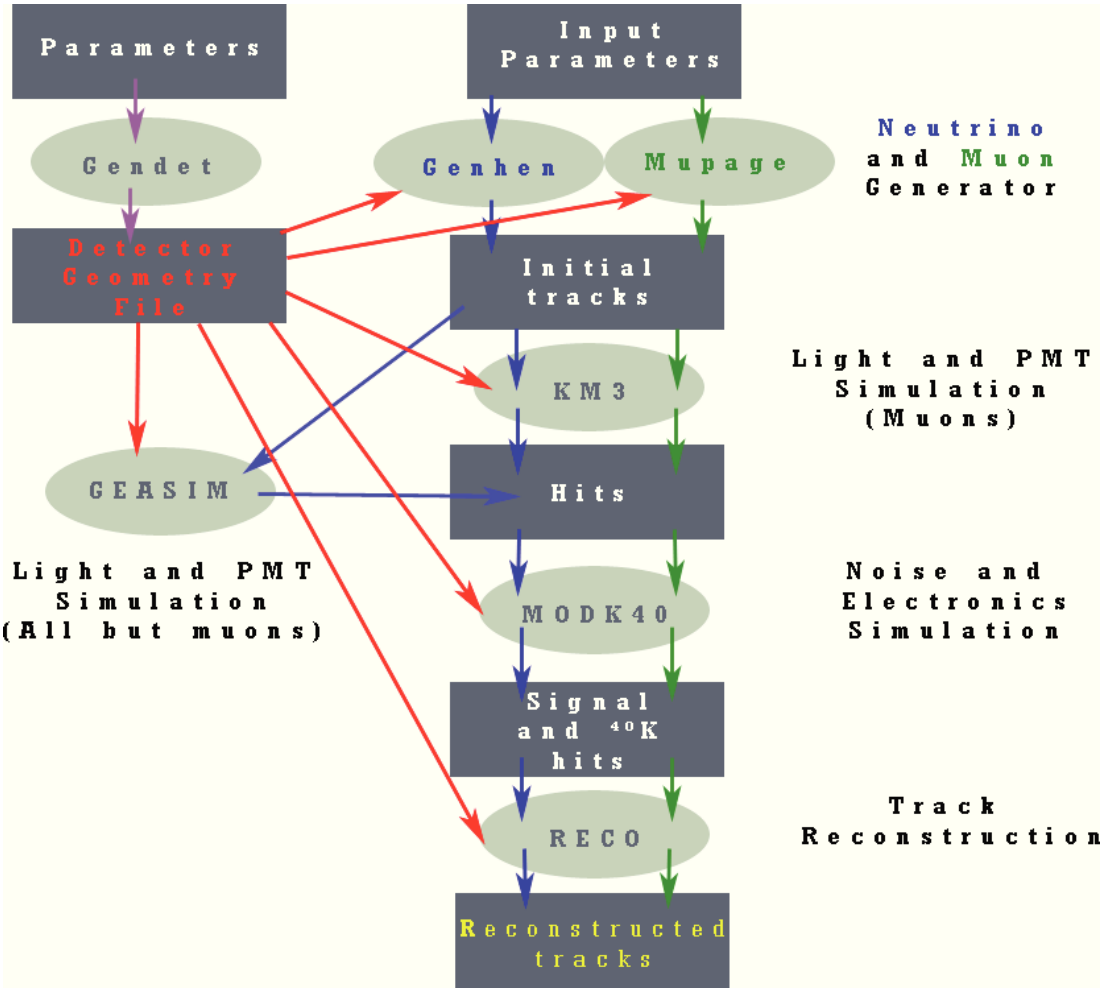

Figure 5.1: Simulation Tools - Simulation Tools Scheme

5.1 GENHEN

The Genhen code is used to generate the neutrino-induced muon flux at the detector. Since the cross-section of the CC interaction is very small simulating all the neutrino events would be disadvantageous in terms in cpu-time. So, the code generates only

neutrinos that interact inside or near the detector and are able to produce detectable muons. The generation volume (V_{gen}) is defined as the volume beyond which a muon has neglectable probability to reach the *can* [1]

The size of V_{gen} strongly depends on the maximum energy of the generated spectrum (E_{max}), on the maximum muon range in water R_w and in rock R_r and on the angular range of the simulation. For a 360° simulation, the generation volume will be a cylinder surpassing the can by R_r in height (for up-going events, $R_w \cos\theta_{max}$ for down-going events) and R_w for the radius.

The interaction vertexes are then uniformly generated inside the scaled V_{gen}. Starting from the vertex, the neutrino direction is generated uniformly in the solid angle (in case of diffuse flux generation) o as a function of the apparent source motion in the detector frame (in case of point-like source generation). The code then simulates the neutrino interaction by means of LEPTO (43) for deep inelastic interaction (DIS) and RSQ (44) for quasi elastic interaction (QEL) and resonant events (RE), giving the cinematics of the produced muons. The muons are eventually propagated up to the can using MUSIC (45), MUM or PropMu.

In the scope of this work, the Genhen code has been modified to allow the generation of neutrinos coming from the Sun. You can find a description of the changes and some reliability tests on this Chapter.

Event Weight

Genhen is able to generate neutrino fluxes with power-law spectrum of chosen spectral index . However, you will hardly deal with pure power-law spectra. Most of the times one wants to evaluate the detector's capability to detect signals from different astrophysical sources with different functions for the neutrino energy spectra. Thus, the procedure we use here (which is of common use) is based on the generation of neutrinos with a pure power-law spectrum of choosen spectral index (ε_ν^{-X}), providing a weight to all the generated events. These events will be re-weighted according to the theoretical expected flux *a posteriori*. This trick frees the simulation work from any link

[1] The *can* (5.2) represents the Čerenkov-sensitive volume, such that photons produced beyond it have neglectable probability to reach a PMT and produce signals. It's the volume around the detector, with height and base bigger by 200m (roughly 3 times the absorption lenght of Čerenkov photons in sea water)

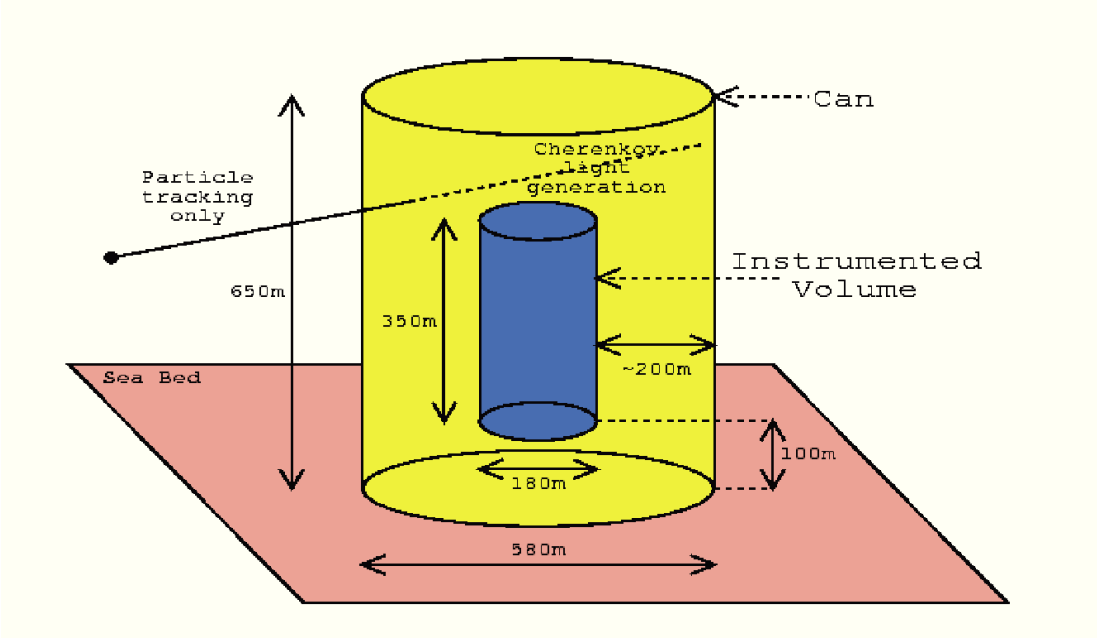

Figure 5.2: The Can - The *can* represents the sensitive volume of the detector

to the particular source (or model) one is considering, granting the chance to compare different models with simple and fast renormalization and weighting procesesses.

In order to allow that, the code assigns a generation weight to each event, defined as the inverse of simulated spectrum:

$$W_{gen} = \frac{1}{(\frac{dn_\nu}{d\varepsilon_\nu dSdt})^{simul}} \tag{5.1}$$

and the event weight is calculated by W_{gen}:

$$W_{eve} = W_{gen}\left(\frac{dn_\nu}{d\varepsilon_\nu dSdt}\right)^{expected} \tag{5.2}$$

The generated energy spectrum, with spectral index X, of the N_{tot} interacting neutrinos is:

$$\left(\frac{dn_\nu}{d\varepsilon_\nu dSdt}\right)^{simul} = \frac{\varepsilon_\nu^{-X}}{I_E} \cdot \frac{N_{tot}}{V_{gen}} \cdot \frac{1}{t_{gen}} \cdot \frac{1}{\sigma_{CC}(\varepsilon_\nu)\rho N_A} \cdot \frac{1}{P_{earth}(\varepsilon_\nu, \vartheta_\nu)} \tag{5.3}$$

I_E being the energy fase factor

$$I_E = \int_{\varepsilon_{\nu,min}}^{\varepsilon_{\nu,max}} E^{-X}\, dE = \begin{cases} \ln \frac{\varepsilon_{\nu,max}}{\varepsilon_{\nu,min}}, & \text{if X = 1} \\ \frac{\varepsilon_{\nu,max}^{1-X} - \varepsilon_{\nu,min}^{1-X}}{1-X}, & \text{if X} \neq 1 \end{cases} \tag{5.4}$$

V_{gen} is the generation volume and t_{gen} the generation time span, i.e. the amount of time the source is below the horizon (we're detecting up-going neutrinos from below) times the simulated days of observation. The term $(\sigma_{CC}(\varepsilon_\nu)\rho N_A)^{-1}$ is the Charged Current(CC) interaction lenght for a neutrino with energy ε_ν, moving in a medium with ρ density and $N_A = 6.022 \cdot 10^{23}\ mol^{-1}$ is the Avogadro number. The term P_{earth} takes into account of the absorption by the Earth of the neutrino, depending on the particle energy, on the crossed medium density and on the lenght of the path. When generating diffuse flux the generation weight is multiplied by the subtended solid angle: $\Omega = 2((cos\vartheta)_{max} - (cos\vartheta)_{min})$.

5.2 MUPAGE

MUPAGE is a quite fast muon generator for neutrino telescopes based on parametric formulas. It is able to treat single and multiple atmospheric muon events. The event kinematics is produced on the surface of a user-defined cylinder, virtually surrounding the detector volume. The flux of muon bundles at different depths and zenith angles, the lateral spread and the energy spectrum of the muons in the bundles are based on parametric formulas obtained according to a specific primary cosmic ray flux model and constrained by the measurements of the muon flux in the MACRO underground experiment.

5.3 KM3

KM3 takes into account all the muon interaction mechanisms with matter (multiple scattering, ionization, bremsstrahlung, couple production, anelastic scattering,...), its energy loss and Čerenkov photons emission, with all the related absorption and diffusion procesesses in the sea water. The produced photons are then propagated to the OMs. Simulating each single photon would take huge CPU time. We avoid that by generating absorption and diffusion photon tables with different photon energies

and then using interpolations on these premade tables. These tables also contain the OM properties and have to be re-calculated for each type of OM that is considered.

Muon propagation inside the can is KM3 task, while the propagation of Čerenkov photons is referred to these premade tables through interpolations.

5.4 GEASIM

GEASIM is a GEANT 3.21 based full simulation propagator and deals with all the products of the neutrino interaction. In this full simulation work KM3 is used as muon propagator and GEASIM has been set to take into account the hadron showers produced at the vertex of interaction. Each shower is treated up to its final products. This detailed particle tracking greatly increases the cputime and it actually has an important role only in the "low" energy range (less then 1 TeV), which is the range of interest for this work. Its average effect is to produce more hits, which are not directly correlated to the muon track . The double-edge effect is that one would expect higher detection rate because of the increased input of hits, but the reconstrucion algorithm should lose reliability dealing with hits not directly related to the muon track (but to secondary products tracks) and thus the angular resolution might get worse.

Anyway this effect changes with the detector geometry and the PMT's characteristics. In last chapter some comparison and results about this effect will be shown.

5.5 MODK40

Once the muon-induced photon hits are stored, MODK40 simply adds the spurious hits due to the undersea optical noise. These time-uncorrelated signals are generated as a Gaussian distribution with selected mean rate depending on the properties of the PMT. They are mainly due to ^{40}K decay and bioluminescence.

^{40}K decays as:

$$^{40}K \rightarrow ^{40}Ca + e^{-} + \bar{\nu}_e \tag{5.5}$$

with a branching ratio of about 89.3%. The produced electron has enough energy (~ MeV) to produce Čerenkov light.

The bioluminesce-related noise is due to the abyssal lifeforms and strongly depends on the sea depths.

It has been deeply studied and measured by ANTARES Collaboration for Toulon site (2000 m depth). The signal rate is made of a 60-120kHz *baseline* with MHz bursts which are likely to be induced by sea currents and seasonal variations. Anyway it is expected to be much smaller at the depths of Capo Passero site (36).

MODK40 also simulates the detector electronics, transforming the photon signals into electric signals, taking also into account electronics and gain noise factors.

5.6 RECO

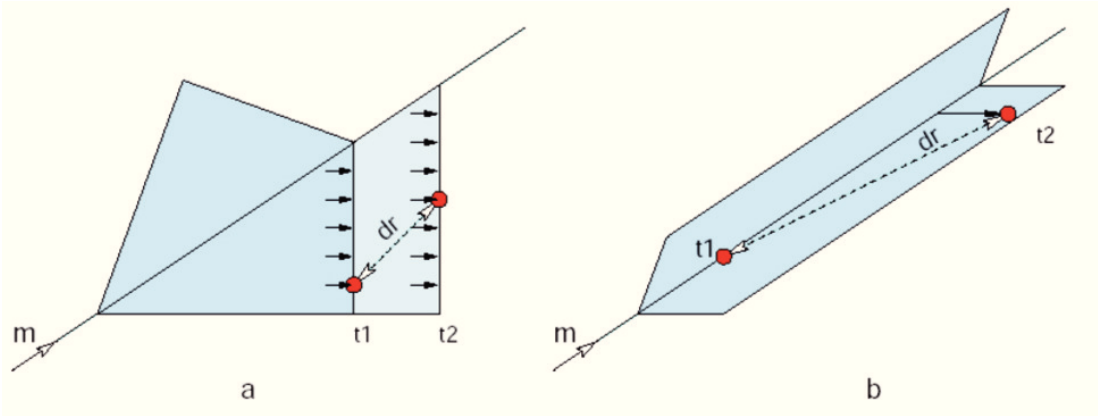

Figure 5.3: Reconstruction algorithm - bla

RECO's aim is to reconstruct the direction of potential event tracks. After a filtering procedure that rejects ^{40}K hits, the track is reconstructed by minimization algorithms. The procedure consists of sequential fitting procedures, using a *trigger*, a *causality filter* and a track reconstruction algorithm.

The trigger is used as first event selection. The trigger condition requires the event to have at least 5 L1-hits (hits in Optical Modules of the same floor within a time window of 10 ns) and 1 OM to contain 3 hits in the same time window of 10 ns.

Then a reference hit is selected, as the first (in time) one of the bundle of hits hitting the optical module having the greatest number of hits amongst all optical modules. The causality filter with respect to the reference hit is applied to all the hits of the event according to the relation:

$$(|dt| - dr/v < 20\ ns) \quad AND \quad (||dt| - dr/c| < 500\ ns) \tag{5.6}$$

where $|dt|$ is the time span between the reference hit and the considered hit, dr is distance between the involved PMTs, v the velocity of the light in water.

The first condition of the (5.6) requires the hits generated within $|dt|$ to be smaller (within 20ns) than the time the Čerenkov wavefront, moving at speed $v = c/n$ ($n \approx 1.35$), takes to cover the distance dr between the two PMTs. The second condition takes into account of the fact that recorded tracks with high dr cannot be generated by photons belonging to the same wavefront beacuse of absorption ($\lambda_a \approx 70$m, with $\lambda = 440$nm). So the hits are to be correlated with respect to the track and the 500ns take into account of the delay in the emission of photons by the muon crossing the detector with speed close to c.

The reconstruction algorithm is eventually applied. It's made of many sequential fits based on minimization functions, whose efficiency has been maximized by the Collaboration. For an exhaustive review on this topic we refer to (42).

Even though neutrino Čerenkov telescopes are optimized to look at muon's tracks coming from below this source of background still holds because the tail of the distribution of misreconstructed tracks extends to high angles, and this effect can be softened only by using track reconstruction quality cuts which will be introduced in the last Chapter.

6

Results

In this chapter we illustrate the results of this work, eventually comparing them with results of other experiments. Firstly, the used strategy is described as well as the different detector layouts introduced earlier in section 4.8. Subsequently, a study on low energy range will be showed with the figures of merit of the detectors. Preliminary sensitivity calculations will also be evaluated and an on-going study on the detector geometries comparison exposed, with special reference to DM detection. Finally, preliminary results on neutrino flux limit from supersymmetric DM annilation into the Sun will be discussed. By this result and under certain assumptions, we will set a limit on the spin-dependent WIMP scattering cross section for some neutralino models.

6.1 Strategy

6.1.1 Events Cuts

At reconstruction level, the Signal-to-Noise Rate (SNR) is always very small, even if we select only events which are reconstructed as upgoing. This effect is mainly due to the atmospheric muons whose trajectories are badly reconstructed as upward tracks.

So we need to introduce some cuts to improve the detector's sensitivity. In order evaluate the detector's performance three reconstruction parameters are used in the analysis of this work:

Λ - related to the quality of the reconstruction;

nHit - represents the number of hits used to reconstruct the event and related to the muon energy;

R_{bin} - used for point-like sources, it is the angular distance between the reconstructed muon's direction and the anti-direction of the chosen source.

Λ cut

Λ is referred to the track reconstruction's goodness. It is defined as:

$$\Lambda \equiv -\frac{\log(L)}{N_{DOF}} \tag{6.1}$$

where L is the reconstruction likelihood and N_{DOF} is the number of degrees of freedom of the fit [1] .

It is known that this quantity is of great importance in disentangling the signal from the atmospheric muon background. The reason becomes clear by comparing figures 6.7 and 6.8.

We claimed above that the number of reconstructed muons at depth of $2 \div 3$ km is still huge compared to that of neutrino-induced muons. Anyway, it sounds sensible that muons (downward) crossing the detector are *badly* reconstructed as *upgoing*, so that their reconstruction Λ (which relates to a likelihood probability) shows a distribution shifted at smaller values than *good* (upward moving) events. Anyway, the tail of the Λ distribution can still affect the SNR in a non-neglectable way.

nHit cut

nHit is the total number of hits recorded for a given event. Obviously, this quantity is sctricly related to energy of the muon, but not directly (Figure 6.1). The number of recorded hits of an event only gives an indication of the energy deposited via Čerenkov

[1] For compatibility issues (waiting for further analysis), we prefer not to use the notation used in many works by ANTARES and NEMO collaborations:

$$\Lambda \equiv -\frac{\log(L)}{N_{DOF}} + 0.1(N_{comp} - 1) \tag{6.2}$$

where N_{comp} is the number of compatible solutions within 1^o given by the reconstruction code, which is known to result in a better valuation of the reconstruction quality. The different reconstruction strategy used for multi-PMTs implies a different evaluation of the correction factor in 6.2

mechanism by the particle and it strongly depends on the muon's rate of energy loss in the medium, on the lenght of the muon track, on the optical background which acts as a bias, on the light absorption in the medium, and so on. Actually, a good energy reconstruction algorithm is still under study. Anyway, we can make use of MC simulations for predictions.

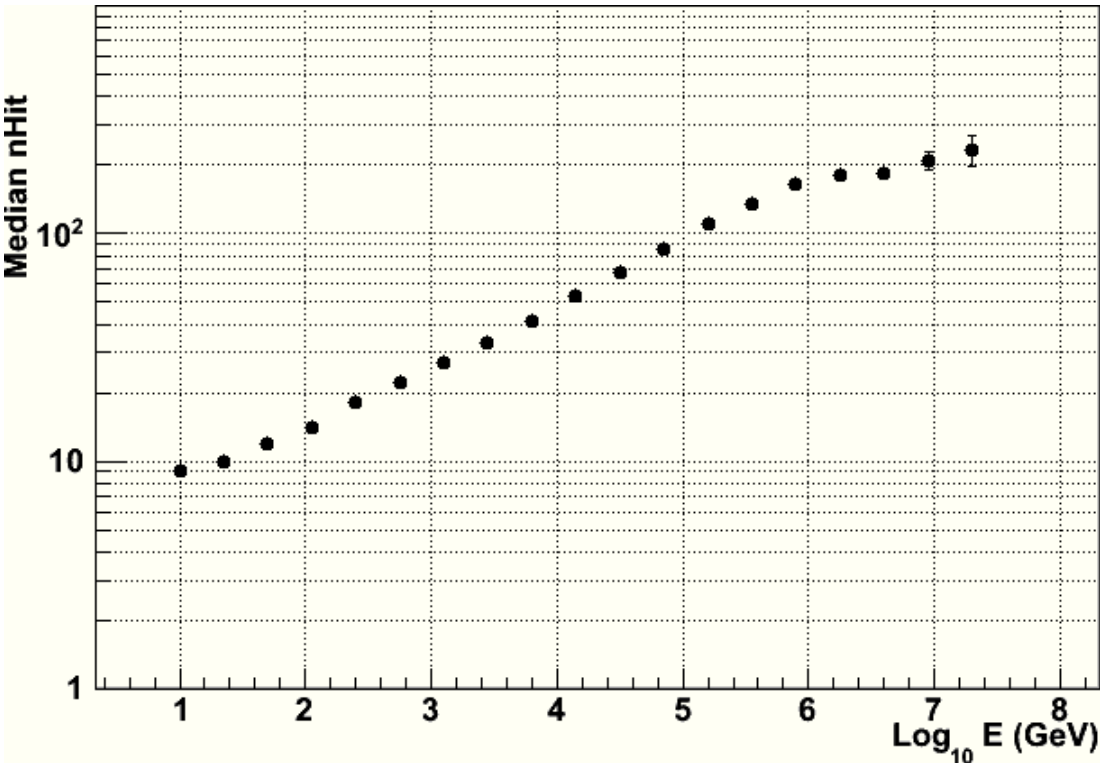

Figure 6.1: nHit Spectrum - The median of the number of hits used in reconstruction procedure after background hits cleanse (nHit) versus the generated neutrino energy E_ν

By plotting the neutrino (generated) energy versus the number of recorded hits (figures 6.2 and 6.4), we can figure out how to use this parameter to properly disentagle signals peaked at different energy ranges.

In particular, requiring events to have at least a minimum number of hits strongly suppresses *low energy* events and spurious background. In fact, a low energy muon will hardly produce a large number of hits along its whole path.

Without a reliable energy reconstruction strategy, it is mandatory to find a good compromise discriminating event signals over both the low energy background and the high energy tail of atmospheric events, especially when the signal is expected to

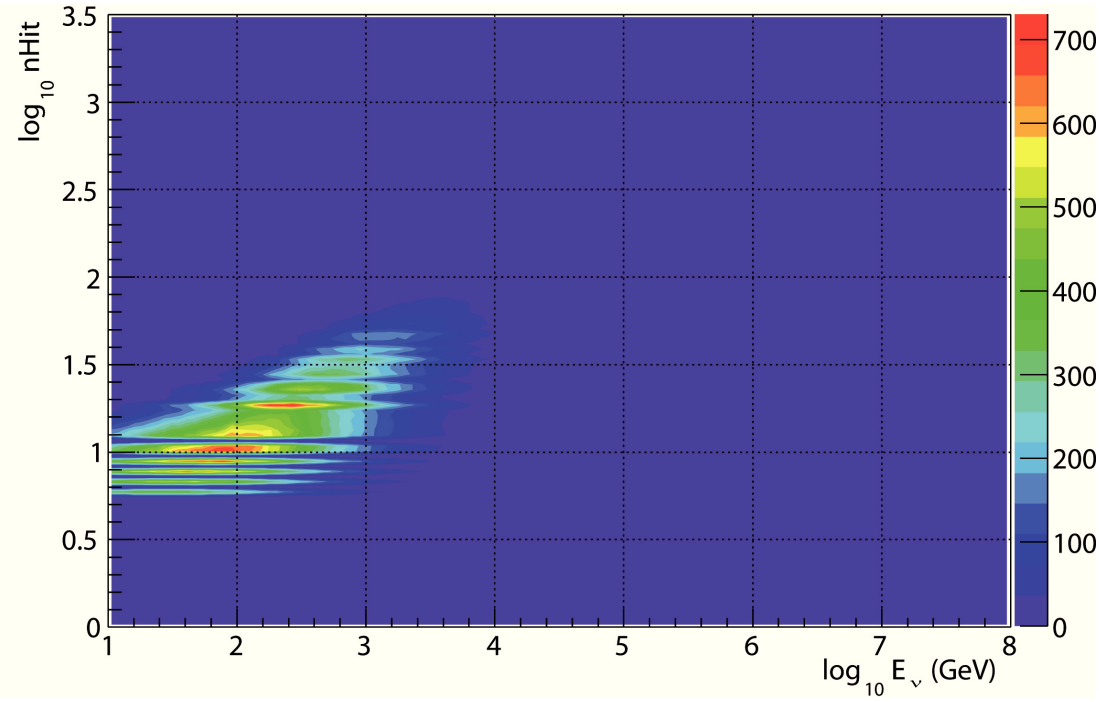

Figure 6.2: Atmospheric nHit - The number of hits per reconstructed atmospheric neutrino event versus the generated energy, at reconstruction level for the *ref*130 layout.

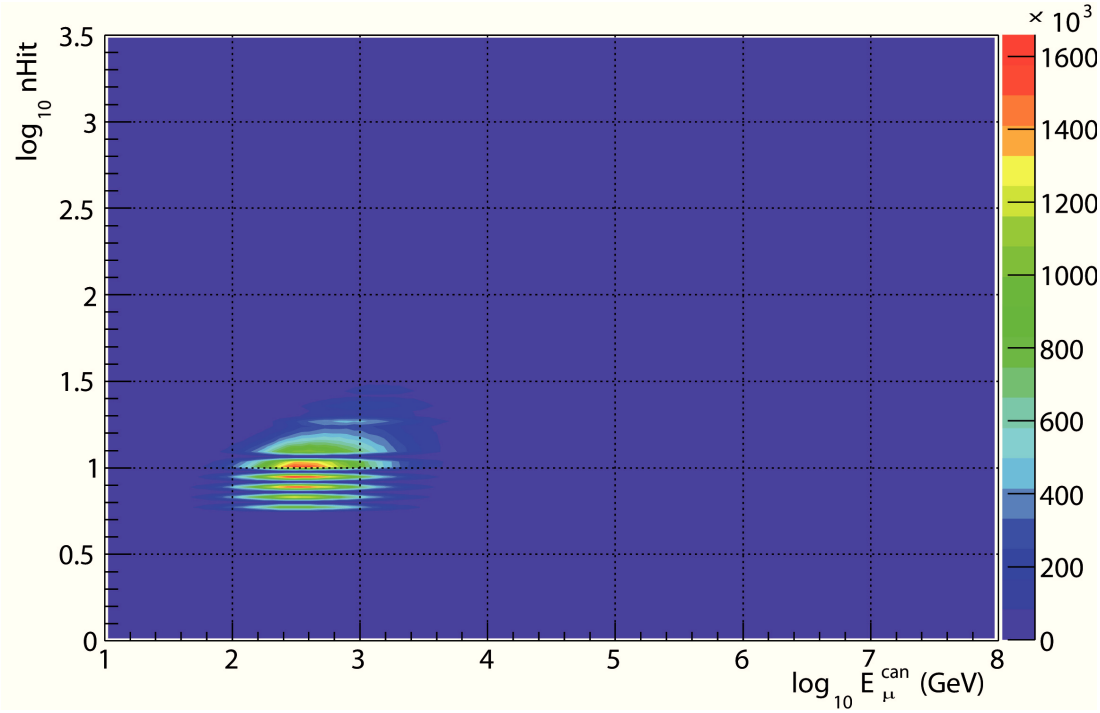

Figure 6.3: Muon nHit - The number of hits per reconstructed atmospheric muon event versus the energy of the muon at the can, at reconstruction level for the *ref*130 layout.

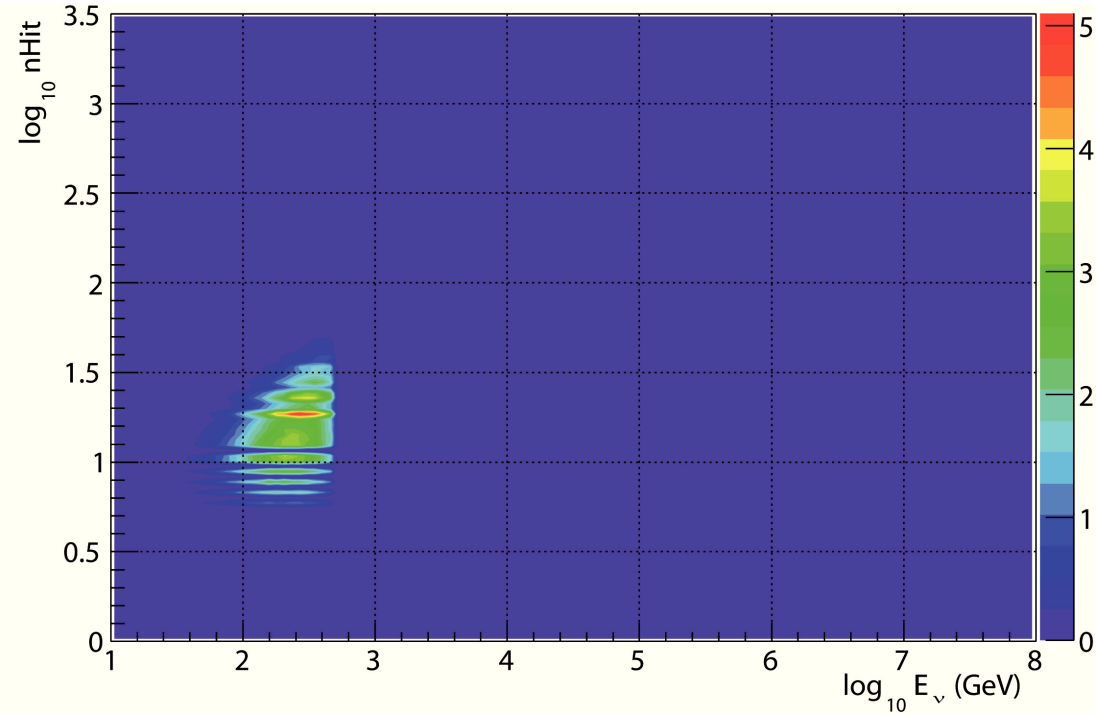

Figure 6.4: Sun nHit - The number of hits per reconstructed signal neutrino event versus the generated energy, at reconstruction level for the *ref*130 layout. The signal refers to 500GeV DM particle annihilating in the Sun through hard channel.

lie in the low energy range. As we can see from figures 6.2, 6.3 and 6.4, by chosing a proper window on the number of recorded hits per event, we can greatly reduce both the low energy background and most of the high energy events which are not related to our signal (atmospheric neutrino background).

R_{bin} cut

When relating to point-like sources, directionality has a very important role in maximizing the SNR. The most intuitive way is to consider a circle centered with the source position and reject all the outer events. Since atmospheric neutrino flux is nearly isotropic, the reduction of the background will go as R_{bin}^2, the smaller the radius of the cone the bigger the reduction.

The choice of the search cone around the source position is ruled by a frail equilibrium between effective area and angular resolution. Obviously enough, shrinking the search bin too much (over the angular resolution of the telescope) will eventually end up rejecting source events as well, backfiring on analysis.

In figure 6.5 the simulated rates (events per year) for atmospheric muon and neutrino fluxes and a reference signal (it refers to a 500 DM annihilating in gauge bosons), expected for the multi-PMT130-204010 detector layout previously introduced (instrumented volume $\sim 1.6 km^3$), are shown. In this (favoured) case the signal is quite strong and after applying some quality cuts altogether one can obtain a distrubion like the one shown in figure 6.6.

6.2 Simulation of the background

For each detector layout described in ref, we generated MC data of atmospheric background. Due to cpu time issues, the data sample are different for each detector but, of course, they are weighted to represent the actual expected background at each detector. If not explicity undermentioned otherwise, the simulation statistics refers to the multi-PMT-130-204010 layout.

6.2.1 Simulation of the neutrino background

The atmospheric neutrino background is a thorn in the side of neutrino Čerenkov telescopes since it's very hard to disentangle from signal. In order to simulate this

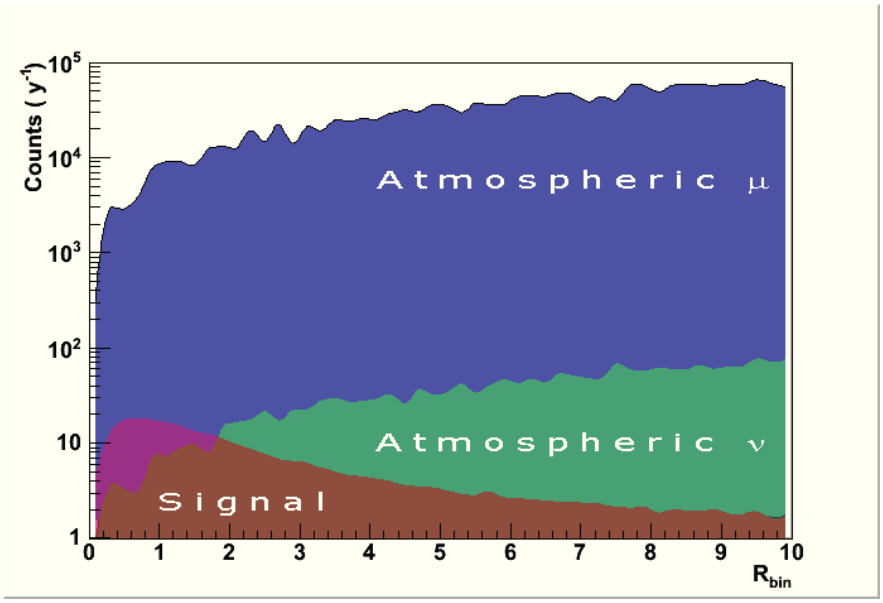

Figure 6.5: R_{bin} - Distribution of reconstructed weighted events with respect to the angular cone size R_{bin}, expected for 1 year of data taking. Without any cuts the rate of atmospheric events overcomes by several orders of magnitude the signal rate, in this plot referred as 500GeV DM particle annihilating in the Sun through hard channel.

background we used the Genhen code with an isotropic generation over 4π solid angle of interacting neutrinos.

About 10^{12} events were generated for each detector's configuration with a -2 spectral index power law spectrum in the energy range $10GeV \div 100PeV$. The events are subsequently weighted using the Bartol parametrization and the RQPM for the prompt neutrino flux (47), to produce a data set of $\sim 10^6$ ref reconstructed events per year at the detector (depending on the detector layouts).

6.2.2 Simulation of muon background

The MUPAGE code is used to generate the atmospheric muon background. It is based on parametrization formulas related to the reference muon flux (46).

In order to grant sufficient total statistics in the energy range of interest for this work, huge cpu time is required. Muon events are generated uniformly in zenith angle $0 \leq \theta \leq 85$, with multiplicity between 1 and 100 at 3500m w.e. depths and a threshold on the muon energy of 1 GeV. The total livetime varies with the detector layout and at

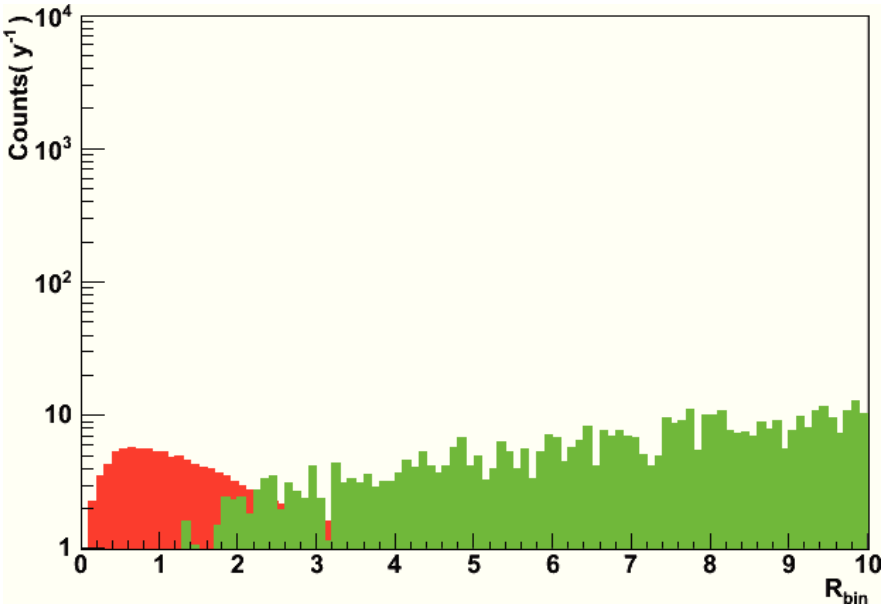

Figure 6.6: R_{bin} **sensicuts** - Distribution of reconstructed weighted events with respect to the angular cone size R_{bin} after the cut strategy, expected for 1 year of data taking. By applying quality cuts on the reconstruction's goodness and on the prediction of the energy range of interest, the rate of atmospheric events is significantly reduced by several orders of magnitude, becoming comparable with the signal rate, in this plot referred as 500GeV DM particle annihilating in the Sun through hard channel.

best it slightly surpasses 24h, despite to very long cpu time consumptions.

We will then assume that for Λ values large enough, the muon background becomes faint and it will be neglected in first analysis (our statistics doesn't provide other choices anyway). This is an optimistic approach but still realistic, forced by the lack of statistics, but supported by the analysis.

In fact, the Λ distributions of muon and neutrino backgrounds are quite different and for $\Lambda \gtrsim -5.5$ the atmospheric muon background is sensitively reduced with respect to neutrino-induced muons, as we can see in figures 6.7 and 6.8.

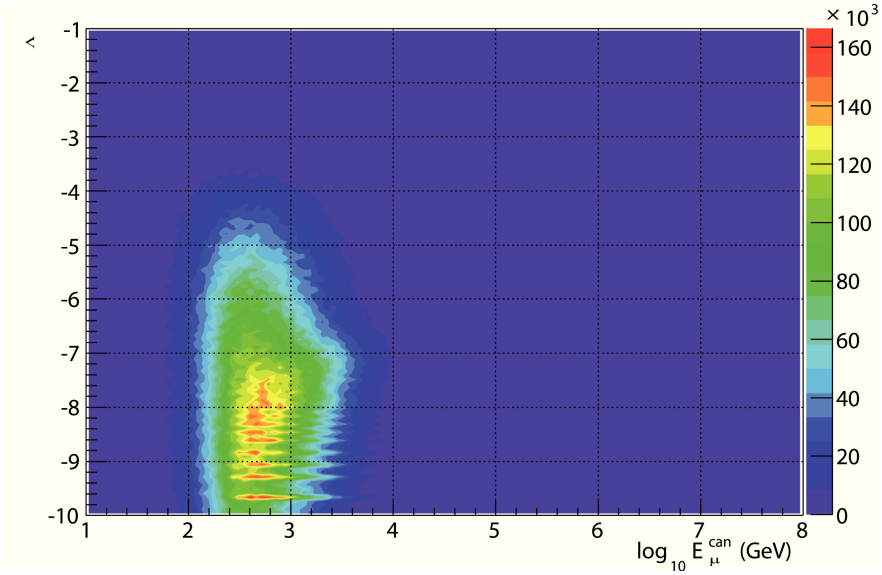

Figure 6.7: Muon Λ Distribution - Λ distribution of upgoing reconstructed muon events in the *ref*130 detector. The distribution is clearly peaked at λ smaller than -7.

6.3 Simulation of neutrino signal from the Sun

6.3.1 Generation of neutrino flux from the sun

In order to use Genhen for generating neutrinos from the Sun we modified the original code. Following the approach used before (4), we added some brand new features to extend its range of usage. In order to compute the Sun position at a given Epoch, we used the well known SLALIB positional astronomy libraries and the results have accuracy of few arcseconds. One can now generate neutrinos coming from the Sun, with respect to the apparent motion of our star in the detector's frame.

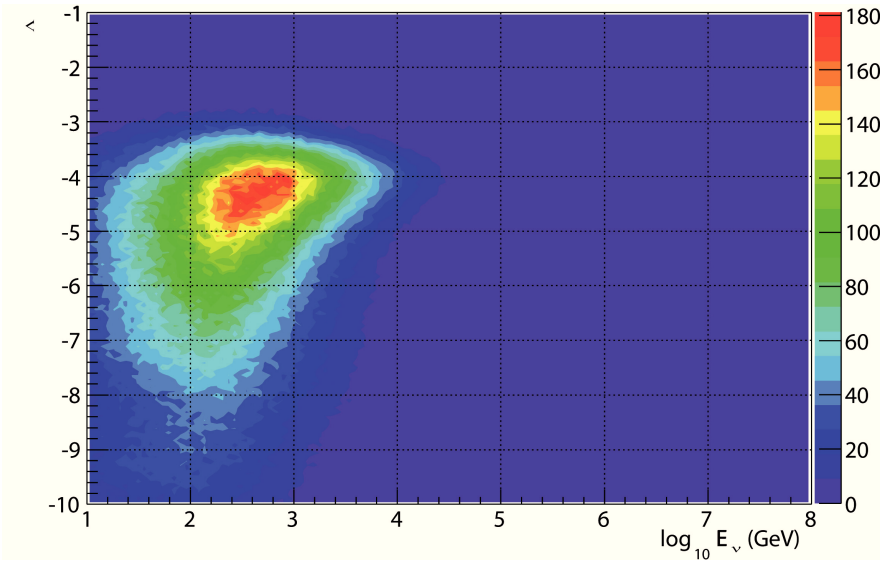

Figure 6.8: Neutrino Λ Distribution - Λ distribution of upgoing atmospheric neutrino reconstructed events. The distribution is clearly peaked at λ greater than -5.

By selecting ”start date” and ”end date” (in Modified Julian Day) of the period of analysis, the code is now able to produce a flux of interacting neutrinos coming from the center of the Sun. The code, which has already been tested by other members of the Collaboration, will be officially released for the Collaboration soon.

The apparent motion of the Sun in the detector's frame is correctly generated. To countercheck the generation procedure, we compared the results with other tools and historical data. The position of the Sun in the frame of Capo Passero site (Latitude 36.27° N, Longitude 16.10° E) calculated by an external tools (50) and the one generated in this work are shown in Figures 6.9, 6.10.

6.4 Detector Layout

In this work we evaluate the performances of tower detector in several configurations for DM annihilation signal's search. The final KM3NeT total number of DUs will be 308, corresponding to two detectors with previously described layouts with 154 towers (or string). Since the results are scalable with DUs number, the results of this work are calculated for 1 detector of 154 towers for a given lifetime or equivalently for 2 detectors of 154 towers referred as *full* detector with half livetime.

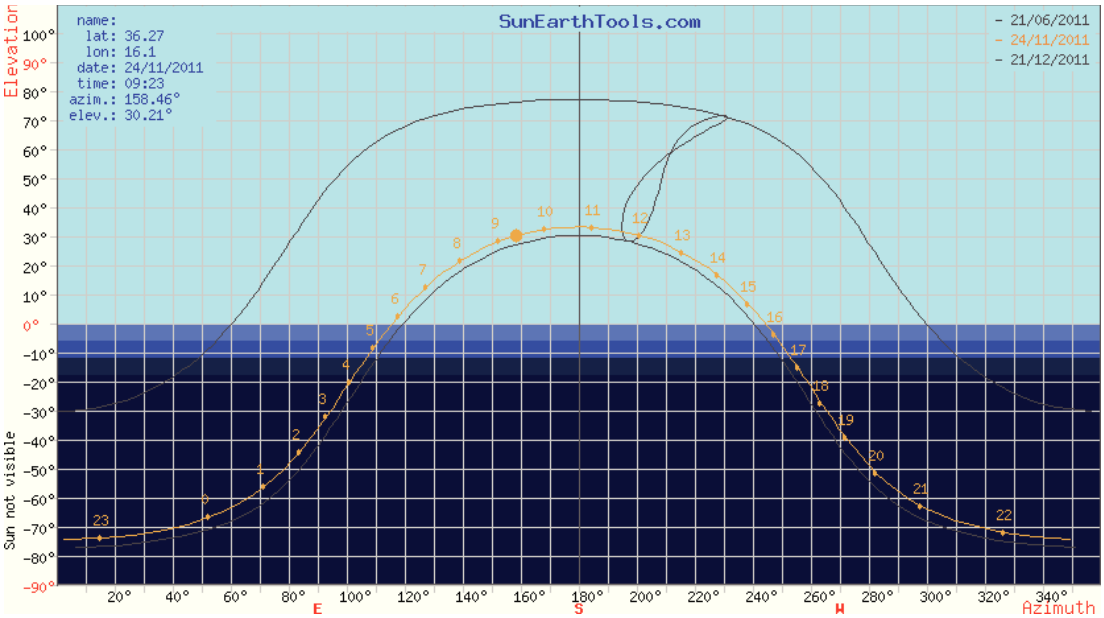

Figure 6.9: Sun Path - The expected *path* of the Sun in the detector frame, reflecting its apparent motion, taken from www.sunearthtools.com

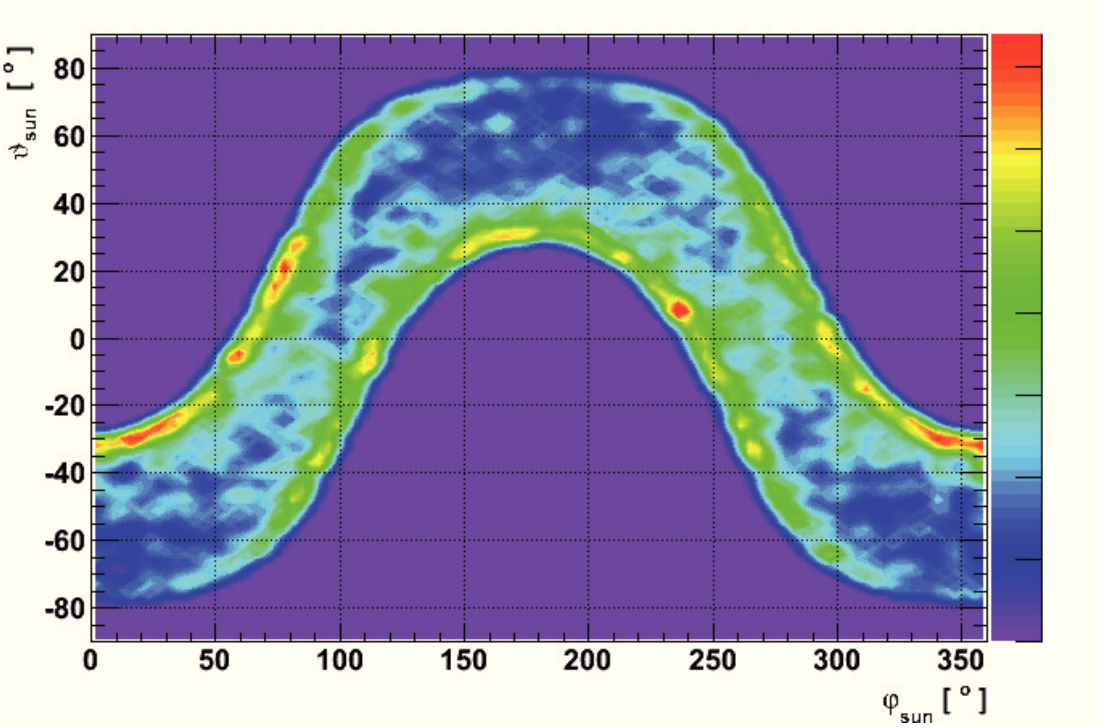

Figure 6.10: Generated Sun Path - The Genhen generated *path* of the Sun in the detector frame, reflecting its apparent motion, used as anti-direction for the generated neutrinos

The three different detector layouts introduced in section 4.8 are described in table 6.1

	nuone154-180204006	**ref154-180204006**	**ref154-130204010**
number of DU	154	154	154
DU height [m]	~ 760 + 100		
DUs spacing [m]	180		130
number of storeys	20		
storeys vertical spacing [m]	40		
storey lenght [m]	6		10
number of OMs per storey	6	2	
number of PMTs per OM	1	31	
size of PMT	8“	3“	
total number of PMTs	18480	190960	
instrumented volume [km^3]	~2.5		~1.6

Table 6.1: Detector Layouts - Characteristics of the detector layouts chosen in this work. The data refer to a single module of 154 towers. The *full* detector is made of two of these modules.

6.4.1 Detector Response

In the low energy range ($E_\nu \lesssim 1TeV$) the light from secondary particles produced at the vertex of the neutrino interaction cannot be neglected and since at this energies a large fraction of events is contanied, it must be taken into account when studying the detector's performance. The GEASIM code (as described in section 5.4) fulfills this task. The effect on the track reconstruction's goodness and on the number of hits belonging to each event will be exploited here. At higher energy this effect vanishes completely since the fraction of contained events is strongly reduced.

In figures 6.11, 6.12, 6.13 the ratios of the recorded hits per event, the effective areas and the angular resolutions are plotted versus the energy of the generated neutrino.

The effective area receives a boost in the $\lesssim TeV$ energy range, at the cost of a slight loss of angular resolution. Anyway this topic needs further investigations which are beyond this work. We will only remark that:

- the effective area increases by a factor of ~1.3 at low energies, figures 6.11;

- as a mirrored effect, the angular resolution increases by a small factor at low energies, figure 6.12;

- the number of the recorded hits at the detector used as input by the reconstructed algorithm is almost the same, figure 6.13;

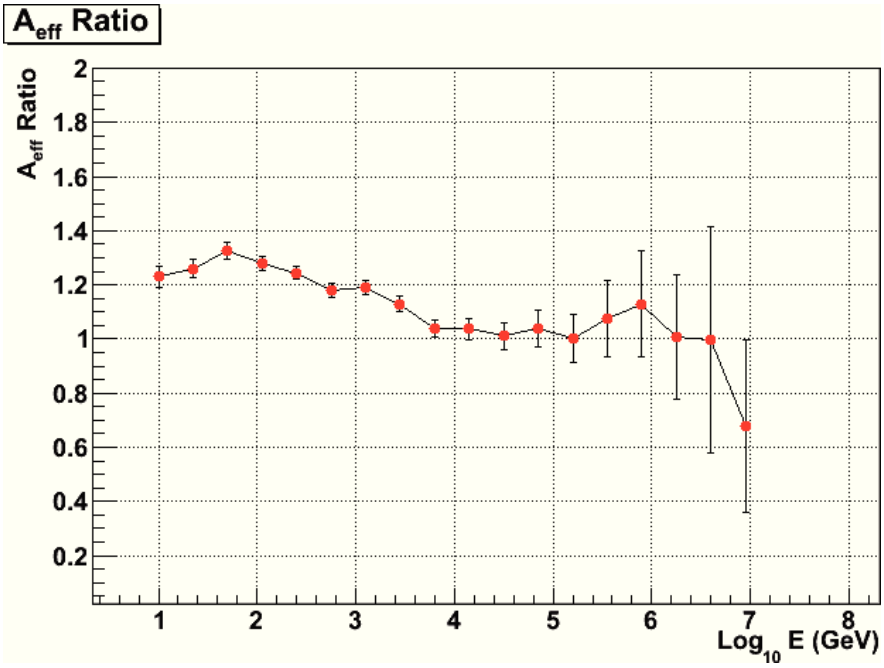

Figure 6.11: GEASIM Aeff - Effective area ratio of GEASIM-included over GEASIM-excluded simulation chains for the *ref*130 layout (upgoing events at reconstruction level)

This effect is not trivial to explain. Secondary particles are supposed to produce a sensitive increase of light, not correlated to the track, if the vertex of interaction is inside the can. A possible solution is that RECO track reconstruction algorithm described in Chapter 5, which uses several minimization procedures, manages to cut most of the hits which are not correlated with the muon track, eventually using nearly the same number of hits for the final reconstruction fit. Anyway the triggering is still higher because of the large local coincidence density caused by this *excess* of light, resulting in a higher rate of successful fitting attempts.

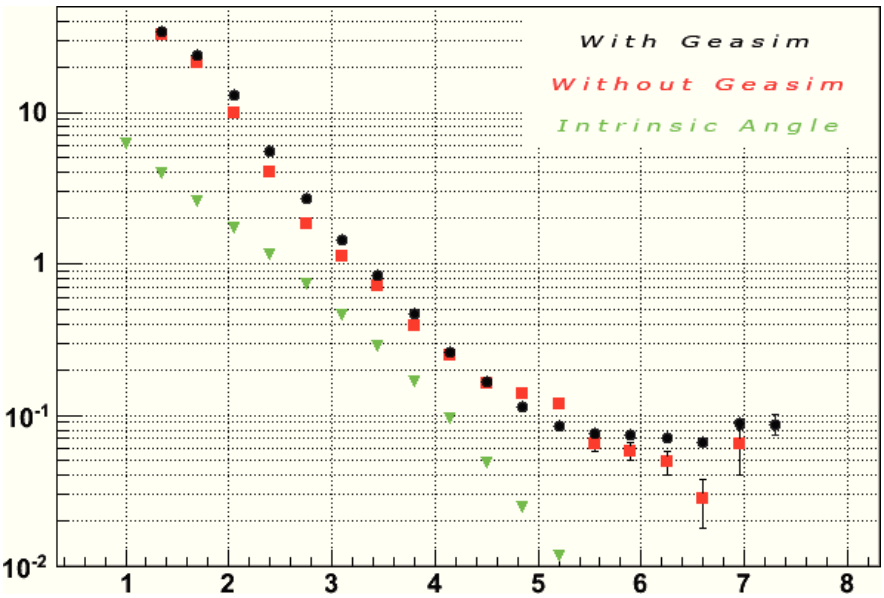

Figure 6.12: GEASIM ang - Angular resolution (median angle) calculated for GEASIM-included (black) and GEASIM-excluded (red) simulation chains for the *ref*130 layout (upgoing events at reconstruction level). For comparison the median of the angle between the neutrino direction and the produced muon is plotted (green)

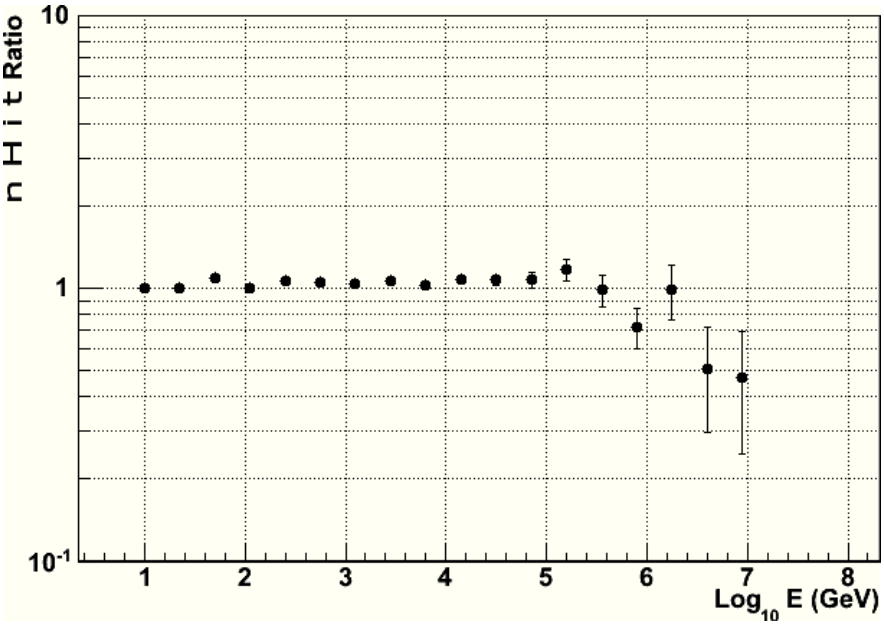

Figure 6.13: GEASIM nhit compare - The ratio of the number of hits used at final steps for the reconstruction strategy is nearly the same for GEASIM-included and GEASIM-excluded simulation chains

6.4.2 Effective Areas

The effective area directly relates a theoretical neutrino flux to the expected event rate in a neutrino telescope and it can be evaluated by means of MC simulations as described in equation 4.6.

In order to select and countercheck our strategy for the quality cuts, we calculate the effective areas and the angular resolution of the detectors with the previously chosen layouts, shown in tab 6.1.

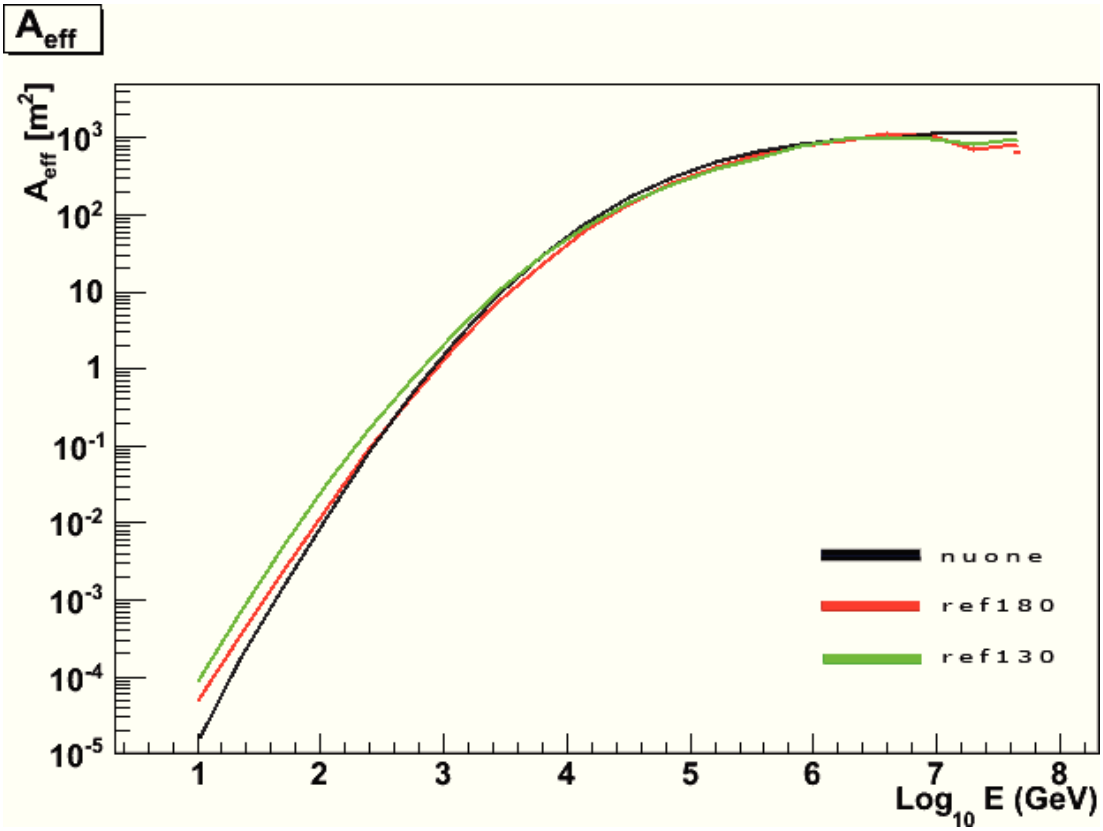

Figure 6.14: Effective Areas - Effective areas of the three detector layouts under study, for the final KM3NeT detector (308 towers). Different quality cuts are applied in order to obtain nearly the same angular resolution in the GeV-TeV range, as shown in figure 6.16.

In figures 6.14, 6.15 the slope of the effective area with respect to the neutrino energy for upgoing events is shown for each considered configuration in the energy range $10GeV \div 100PeV$, for the final KM3NeT detector (308 towers). Events selection criteria are applied in order to grant comparable angular resolution at hundreds of

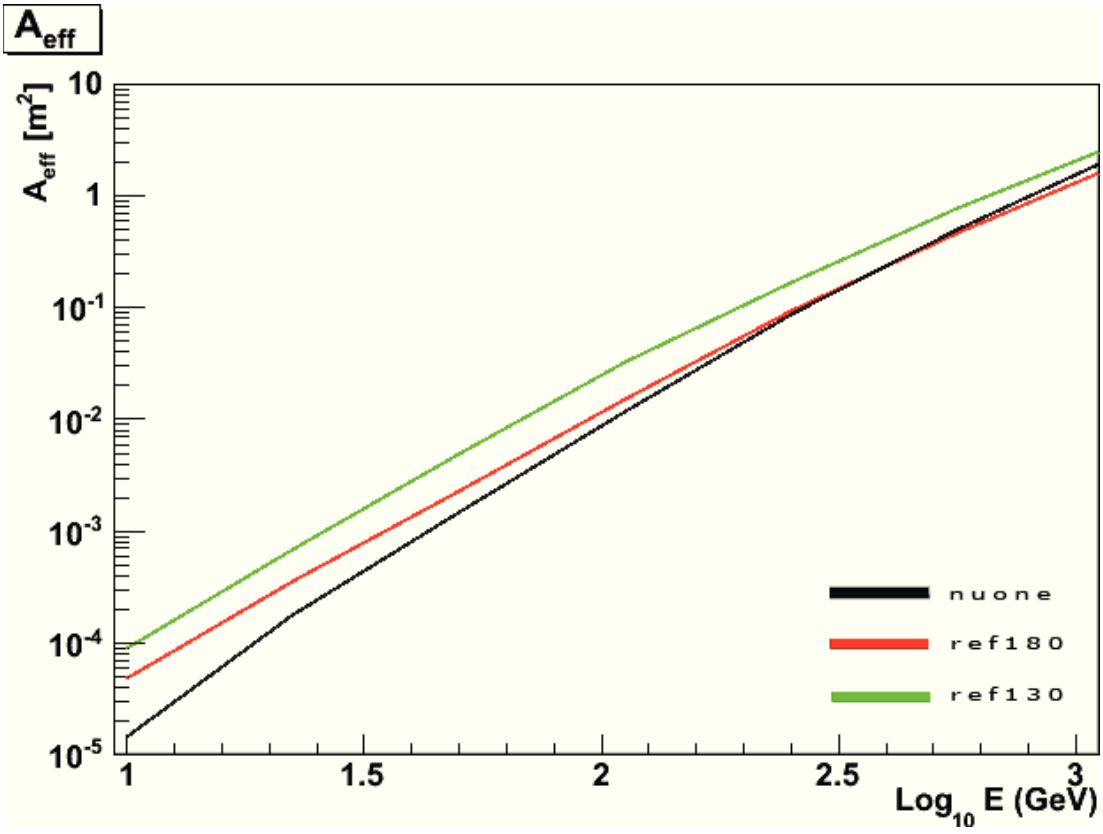

Figure 6.15: Effective Areas Zoom - Close-up of the energy range of interest of the effective areas of the three detector layouts under study, for the final KM3NeT detector (308 towers). Different quality cuts are applied in order to obtain nearly the same angular resolution in the GeV-TeV range, as shown in figure 6.16

GeVs.

Effective areas increase very quickly in the range 10 GeV - 1 TeV ($cm^2 \div m^2$) and almost linearly with the logarithm of the energy up to the PeV region, after which becoming nearly saturated at few km^2.

The effect of multi-PMT at low energies is clear. The multi-PMT with 130m DU spacing and 10m bar grants a significant boost in both effective area and angular resolution at the energy of our interest ($10GeV \div 1TeV$). This is quite probably due to the double effect of the tower narrowing and the multi-PMT which both greatly increases PMTs local density.

6.4.3 Median angles

The angular resolution of a neutrino underwater telescope grants the possibility to effectively choose the proper events cut criteria to minimize the background.

As anticipated above and as it can be seen in figures 6.16, 6.17, the multi-PMT detector with 130m DU spacing grants better angular resolution yet holding an increased effective area effect as well.

For this reasons this layout is likely to be the golden configuration amongst the ones considered.

6.5 Neutrino flux from DM annihilation in the Sun

In Chapter 3 we introduced the neutrino spectra produced by each of the DM annihilation channels and in chapter ref we showed the weight procedure. Here we will discuss the spectra of corresponding reconstructed tracks.

We chose two annihilation channels in order to compare this work's results with those of other neutrino telescopes (ANTARES, IceCube), but this method can be easly applied to all the channels. The W^+W^- channel is referred as "hard" spectrum and the $b\bar{b}$ as "soft" one. The $\tau^+\tau^-$ channel which can produce hard flux will be part of our analysis as well.

The weighting proceure of 5.2 allow us to test different models, providing specific fluxes.

The spectra of reconstructed events using the flux in 3.5 and 6.3 we have the rate of reconstructed event at detector per year for the specific theoretical flux at detector:

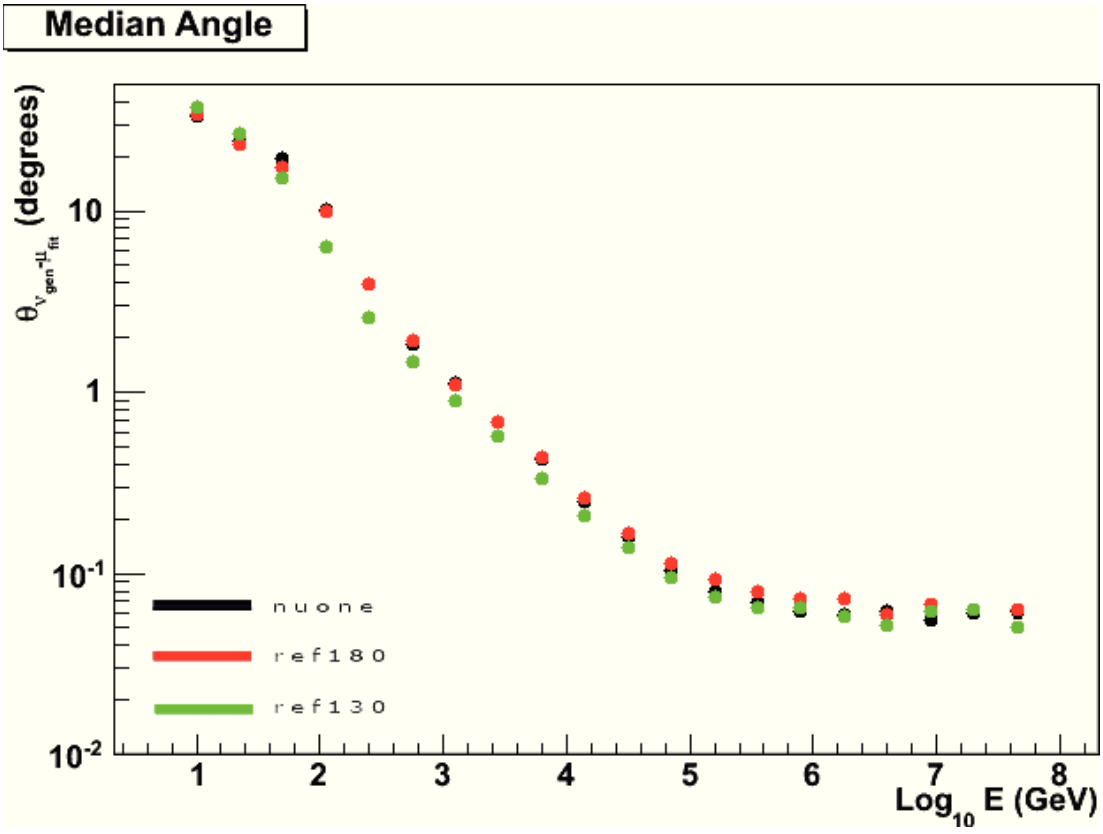

Figure 6.16: Median Angle - Angular resolution of the three detector layouts under study, for the final KM3NeT detector (308 towers). Different quality cuts are applied in order to obtain nearly the same angular resolution in the GeV-TeV range, for comparing effective areas as in figures 6.14, 6.15.

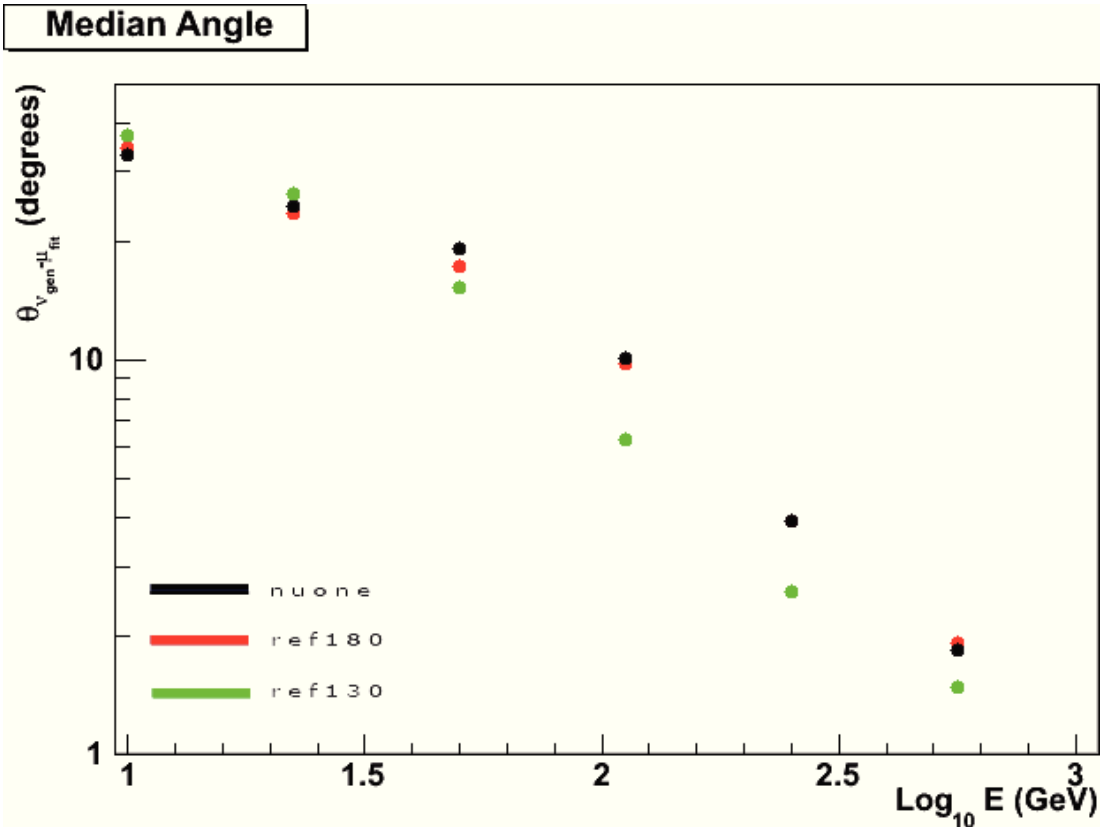

Figure 6.17: Median Angle Zoom - Close-up of the angular resolution slope of the three detector layouts under study, for the final KM3NeT detector (308 towers). Different quality cuts are applied in order to obtain nearly the same angular resolution in the GeV-TeV range, for comparing effective areas as in figures 6.14, 6.15.

$$R_{det}(years^{-1}) = \int A^{\nu}_{eff}(E_\nu, \theta_\nu) \frac{d\phi_\nu(E_\nu, \theta_\nu)}{dE_\nu} \tag{6.3}$$

Different models, thus different neutrino fluxes ϕ_ν, will produce different event rates at detector. In our analysis we separately assume BR=1 for the considered channels and arbitrarily use:

$$\Gamma_A = \frac{10^{14}}{sec} \left(\frac{100GeV}{m_{WIMP}} \right)^2 \tag{6.4}$$

as reference flux normalization factor for our sensitivity calculation.

We consider m_{WIMP}={300 GeV, 500 GeV, 1TeV} and the channels:

$$\chi\chi \rightarrow b\bar{b} \tag{6.5}$$

$$\chi\chi \rightarrow W^+W^- \tag{6.6}$$

$$\chi\chi \rightarrow \tau^+\tau^- \tag{6.7}$$

6.5.1 Reconstructed Spectra

In figures 6.18, 6.19 and 6.20 the spectra of the reconstructed weighted (according to the above procedure) events are shown, for different channels and DM mass, for the three layouts.

In figure 6.21 an example of the reduction on the data set due to the applied strategy cuts is shown.

6.6 Event Rate

By using equation 4.8 and the provided fluxes (5) we can calculate the telescope sensitivity for each given DM model of our analysis. In table 6.2 the models used in this work are listed, with the upgoing reconstructed weighted events of each model by 5.2 , before any optimisation events cuts.

6.7 Sensitivity

The neutrino differential flux sensitivity refers to the average upper limit μ_s^{90} on the differential neutrino flux for an ensemble of experiments with zero expected signal events.

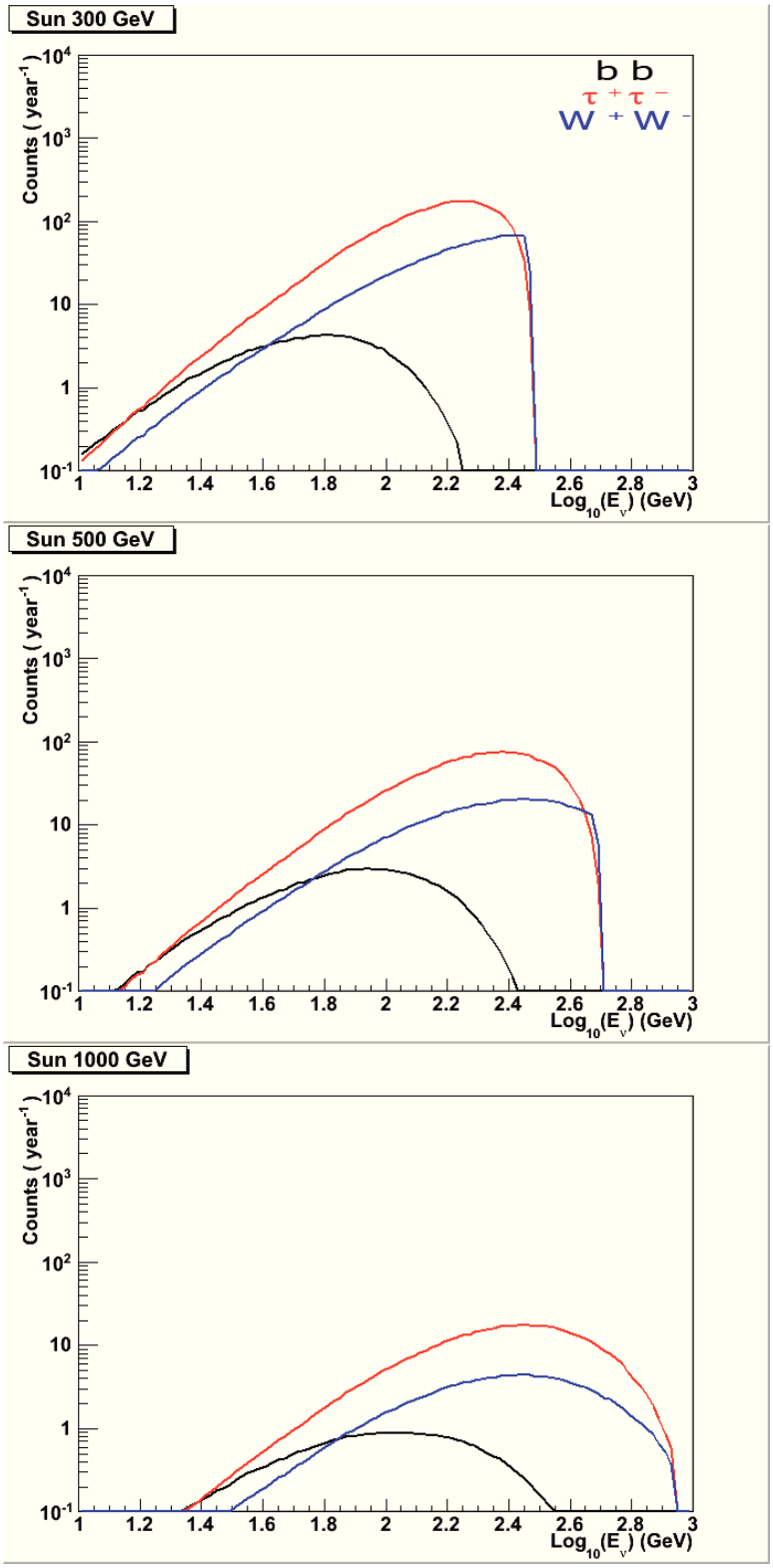

Figure 6.18: ref130 spectra - Spectra of reconstructed events in the *ref*130 layout detector for 300GeV, 500GeV and 1TeV DM particle annihilating in selected channels, normalized to 1 year.

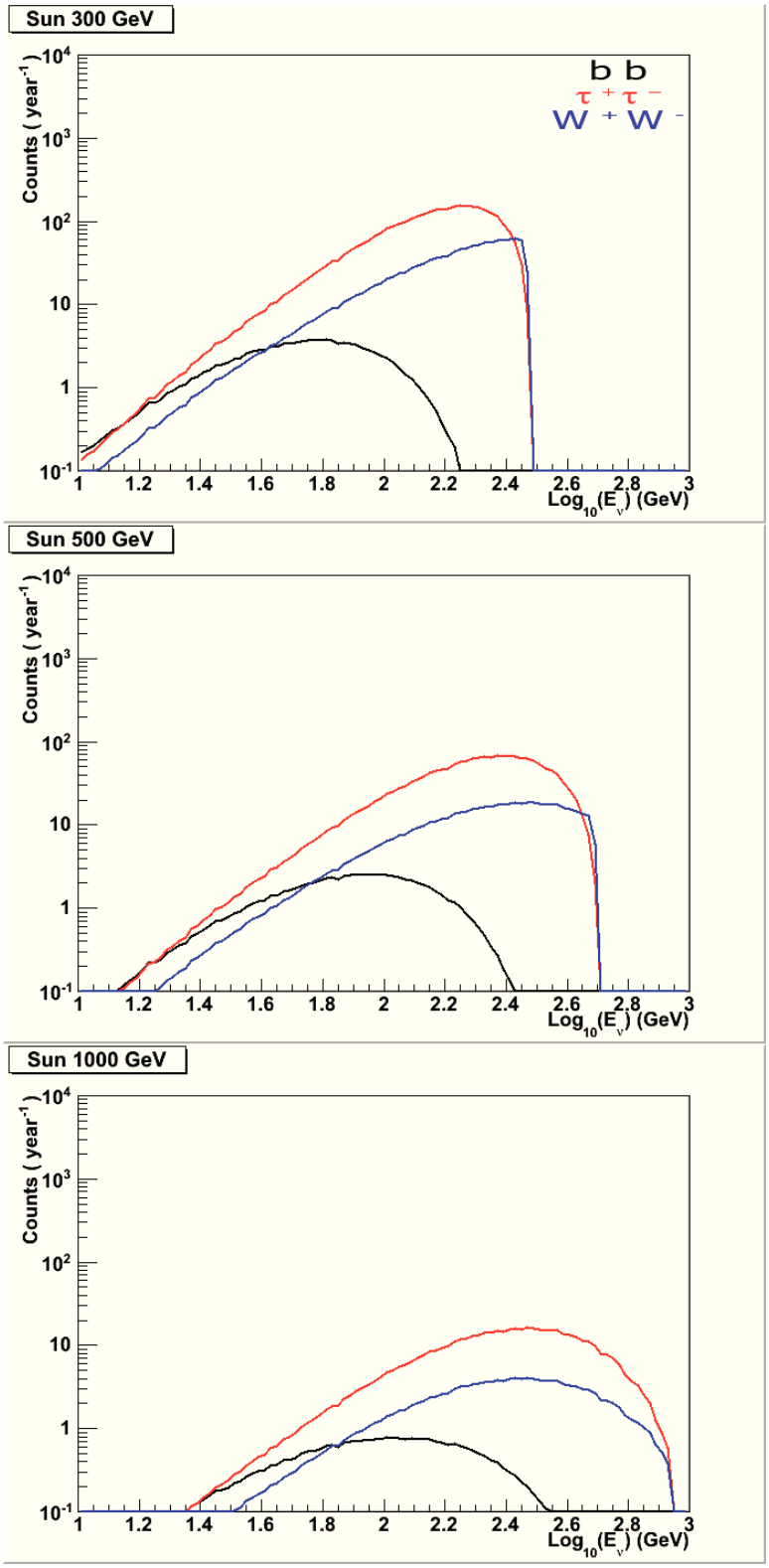

Figure 6.19: ref180 spectra - Spectra of reconstructed events in the *ref*180 layout detector for 300GeV, 500GeV and 1TeV DM particle annihilating in selected channels, normalized to 1 year.

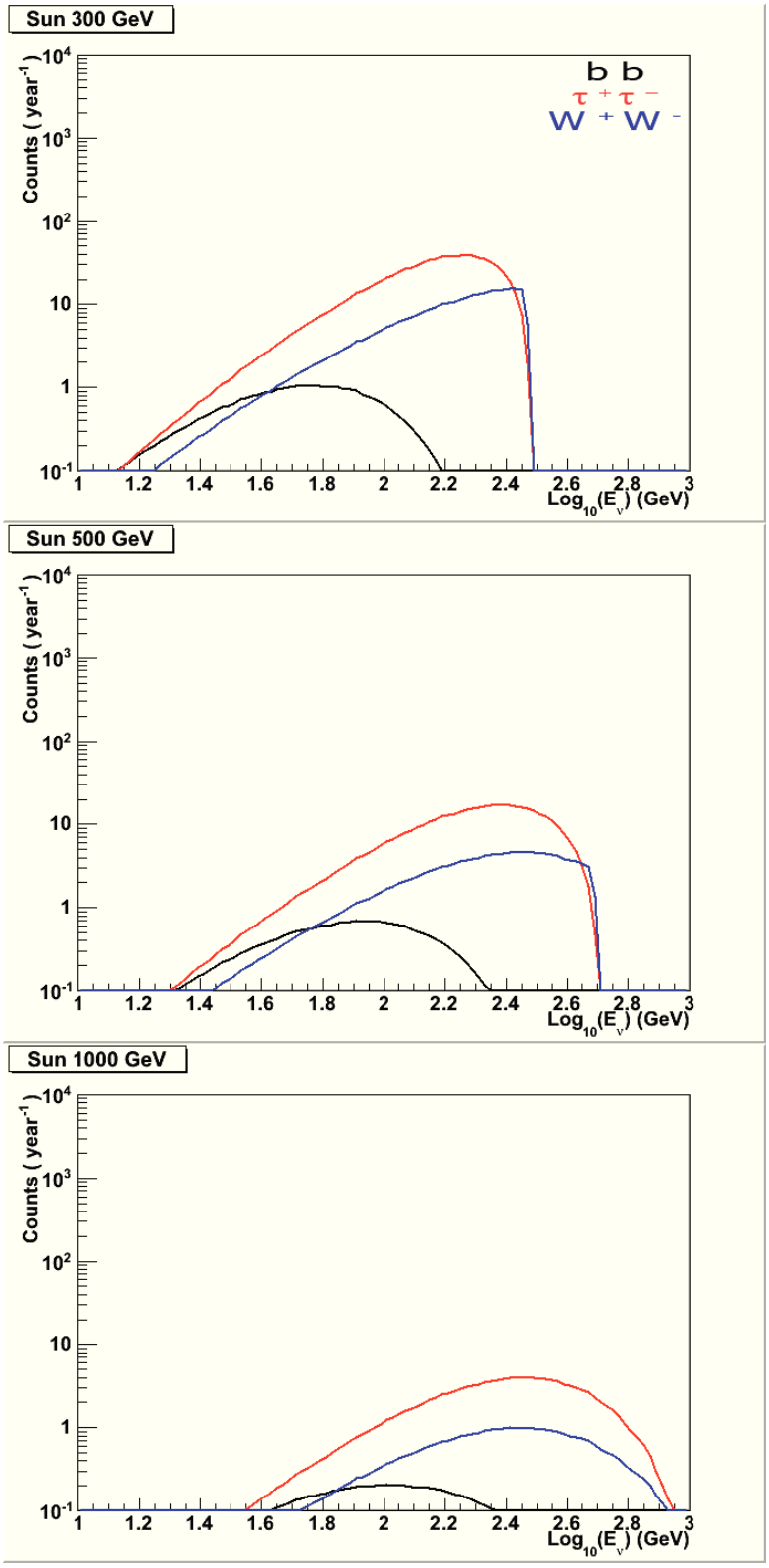

Figure 6.20: nuone180 spectra - Spectra of reconstructed events in the *nuone*180 layout detector for 300GeV, 500GeV and 1TeV DM particle annihilating in selected channels, normalized to 1 year.

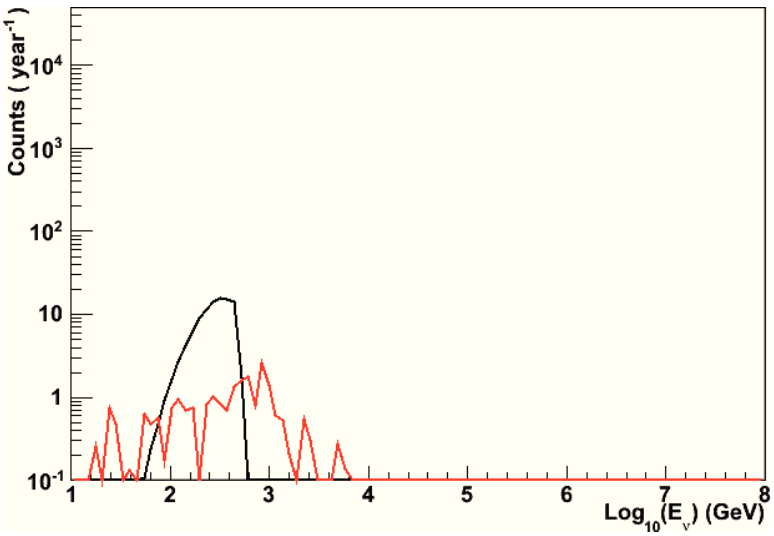

Figure 6.21: sun500cuts ref130 - Spectra of reconstructed events in the *ref*130 layout detector for 500GeV DM particle annihilating in *hard* channel after sensitivity cuts, normalized to 1 year

		Reconstructed Events(year^{-1})		
DM Mass(GeV)	Channel	**nuone**	**ref-180**	**ref-130**
300	$b\bar{b}$	32.0301	113.101	126.445
300	$\tau^+\tau^-$	874.684	3354.59	3835.94
300	W^+W^-	309.777	1198.44	1359.61
500	$b\bar{b}$	22.3594	81.3308	92.3877
500	$\tau^+\tau^-$	450.101	1762.37	1978.06
500	W^+W^-	138.899	546.742	607.904
1000	$b\bar{b}$	7.76035	28.7704	32.6728
1000	$\tau^+\tau^-$	124.727	495.777	545.445
1000	W^+W^-	34.1967	135.704	149.21
Atm $\nu + \bar{\nu}$		4.4E+5	3.4E+5	3.6E+5
Atm μ		6.1E+08	2.5E+08	1.7+08

Table 6.2: Expected upgoing event rate for the three layouts, for the signal in all the considered models and the background, in 1 year of data taking before event cuts, weighted with 6.3 and 6.4. The expected backgrounds events weighted according to the chosen parametrization are showed as well.

A multi-parametetric algorithm, based on the strategy discussed before in ref, is used in order to minimize the sensitivity to DM signals. The results are summarized in tables 6.3 for 1 year of data taking and 6.4 for 5 years.

		Sensi$^{90}(GeV^{-1}sec^{-1}m^{-2})$		
DM Mass(GeV)	Channel	**nuone**	**ref-180**	**ref-130**
300	$b\bar{b}$	1.82	1.05E-1	5.35E-2
300	$\tau^+\tau^-$	1.26E-2	1.13E-3	5.09E-4
300	W^+W^-	2.82E-2	2.64E-3	1.23E-3
500	$b\bar{b}$	4.71E-1	3.48E-2	1.51E-2
500	$\tau^+\tau^-$	5.50E-3	5.20E-4	2.59E-4
500	W^+W^-	1.59E-2	1.49E-3	7.72E-4
1000	$b\bar{b}$	2.07E-1	1.71E-2	7.69E-3
1000	$\tau^+\tau^-$	3.77E-3	3.53E-4	1.91E-4
1000	W^+W^-	1.39E-2	1.29E-3	7.08E-4

Table 6.3: Expected sensitivity for the three layouts and all the considered models after 1 year of full detector data taking

By integrating 4.8 one can derive the 90% confidence level limit on the neutrino events rate from DM annihilating into the Sun which can be used for comparison with other experiments.

6.8 Annihilation rate and Cross-section

We saw in Chapter 3 that the capture rate C_C and the annihilation rate are related in equilibrium[1] as $\Gamma_A = C_C/2$ and that the capture rate is strictly related to the neutralino-proton scattering cross-sections σ^{SI} and σ^{SD}.

Under the hypothesis that the capture rate is fully dominated either by spin-dependent ($\sigma_{tot} \simeq \sigma^{SD}_{\chi-H}$) or spin-independent ($\sigma_{tot} \simeq \sigma^{SI}_{\chi-H} + 0.07\sigma^{SI}_{\chi-He} + \ldots$) scattering, we can simply relate the annihilation rate to either the SD or the SI neutralino-proton cross setion. More details on calculations can be also found in (54),(55).

Under this assumption, setting an upper limit over the neutrino flux from DM annihilation in the Sun translates into a limit for its annihilation rate as it is defined in

[1]Equilibrium has been achieved in the Sun for many DM models including neutralino, (5)

		Sensi^{90}(GeV$^{-1}sec^{-1}m^{-2}$)		
DM Mass(GeV)	Channel	**nuone**	**ref-180**	**ref-130**
300	$b\bar{b}$	5.33E-1	3.18E-2	1.52E-2
300	$\tau^+\tau^-$	3.60E-3	3.24E-4	1.43E-4
300	W^+W^-	8.04E-3	7.49E-4	3.53E-4
500	$b\bar{b}$	1.37E-1	1.02E-2	4.26E-3
500	$\tau^+\tau^-$	1.57E-3	1.45E-4	7.41E-5
500	W^+W^-	4.54E-3	4.12E-4	2.21E-4
1000	$b\bar{b}$	5.88E-2	4.92E-3	2.16E-3
1000	$\tau^+\tau^-$	1.07E-3	9.64E-5	5.48E-5
1000	W^+W^-	3.93E-3	3.52E-4	2.02E-4

Table 6.4: Expected sensitivity for the three layouts and all the considered models after 5 years of full detector data taking

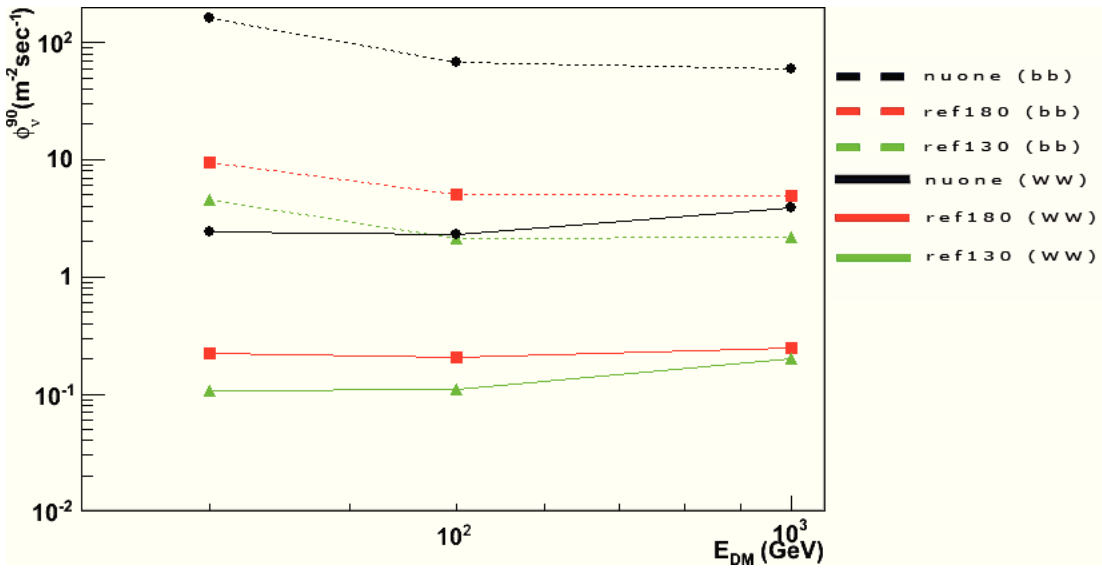

Figure 6.22: Sensitivity - Expected sensitivity for the three layouts (in different coloured lines) and all the considered models and channels (hard channel in solid lines, soft channel in dotted lines) after 5 years of full detector data taking

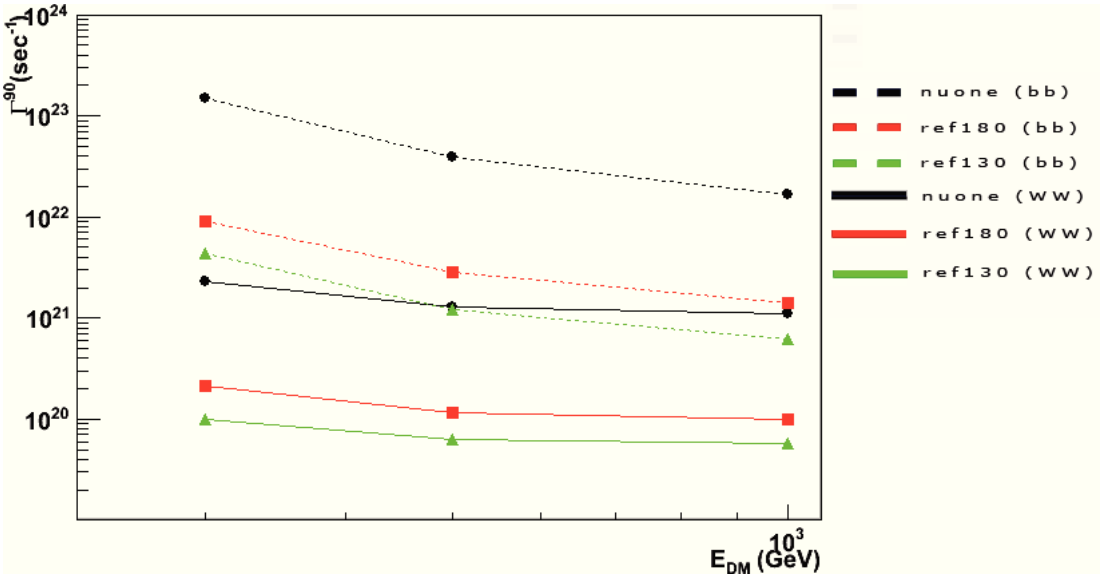

Figure 6.23: Annihilation Rate - Expected limit for the annihilation rate for the three layouts (in different coloured lines) and all the considered models and channels (hard channel in solid lines, soft channel in dotted lines) after 5 years of data taking

3.5.

In figure 6.23, the expected limits on WIMP annihilation rate for 300GeV,500GeV and 1000 GeV DM particles annihilating into the Sun through the "soft" and "hard" channelsare shown.

Also, at equilibrium, equation 3.4 relates annihlation rate and capture rate which, in turn, is defined in 3.1 under general assumptions.

The upper limits for neutrino flux, annihilation rate and SD cross-section calculated for 300GeV, 500GeV and 1000 GeV DM particles annihilating into the Sun through the "soft" and "hard" channels previously defined are shown in tables 6.3, 6.4 and in figures 6.22, 6.23 and 6.24.

Comparing KM3NeT sensitivity to DM signals with other results (Figure 6.24) requires prudence.

KM3NeT limits to SD cross-section is expected to provide exceptional insights on Supersymmetric DM models, providing the chance to inspect the parameter space to a great extent, but these results have yet to be confirmed.

Comparing these results with other experiments (e.g.: IceCube (56), (57)) as shown in figure 6.24, proves full KM3NeT's expected sensitivity to spind-dependent cross-

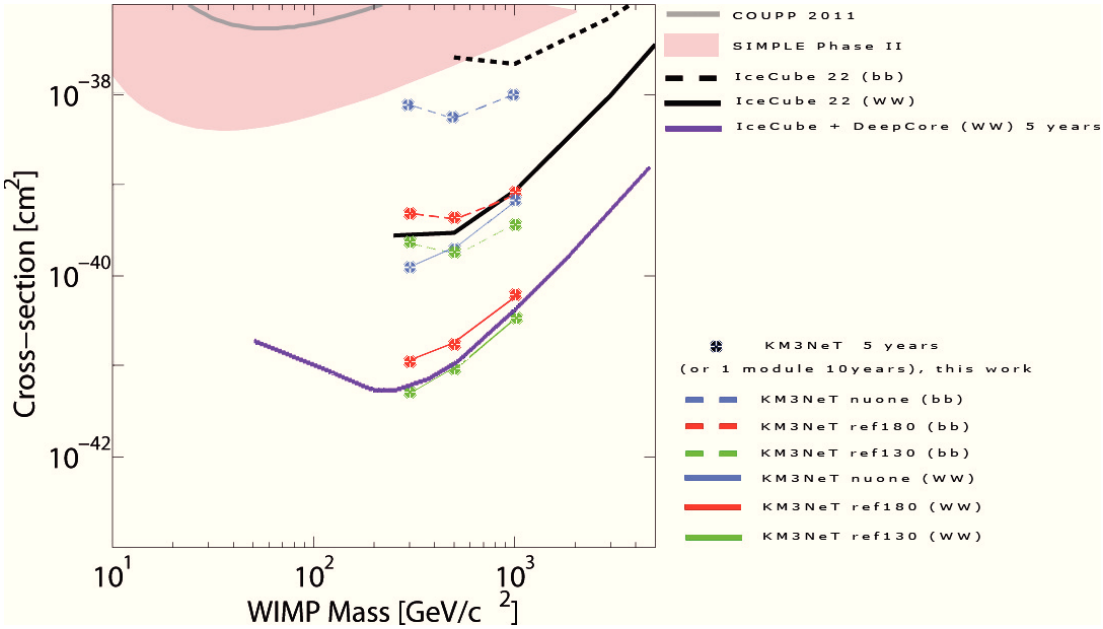

Figure 6.24: σ_{SD} **Limits** - σ_{SD} Spin-dependent cross section limits for different experiments as shown in the legend on the left. COUPP and SIMPLE-*II* limits are from from direct search. IceCube with 22strings limits for hard (black solid) and soft (black dashed) channels are shown as comparison with KM3NeT along with the 5 years expected IceCube 80 strings with DeepCore extension (6 compact strings) limit for the hard channel (violet. The 5 years limits for KM3NeT detector in three possible configurations are shown for the soft (dashed line) and hard (solid line) channels. Different colors relate to different detector's layouts, as described in the legend on the left.

DM Mass(GeV)	Channel	$\Gamma_A^{90}(year^{-1})$	σ_{SD}^{90}
300	$b\bar{b}$	4.30E+21	2.31E-40
300	$\tau^+\tau^-$	4.04E+19	2.00E-42
300	W^+W^-	9.98E+19	5.00E-42
500	$b\bar{b}$	1.20E+21	1.80E-40
500	$\tau^+\tau^-$	2.10E+19	3.00E-42
500	W^+W^-	6.25E+19	9.00E-42
1000	$b\bar{b}$	6.11E+20	3.65E-40
1000	$\tau^+\tau^-$	1.55E+19	9.00E-42
1000	W^+W^-	5.71E+19	3.40E-41

Table 6.5: Annihilation rate and spin dependent cross-section upper limits for 5 years of data taking (full detector), for the ref154-130204010 and three selected channels and DM mass.

section for DM annihilating into the Sun to be comparable to (slighlty better than) the expected IceCube+DeepCore limits, after the same years of data taking (5 years), surpassing the current limits coming from direct detection experiments by orders of magnitudes.

Anyway, it is clear by this analysis that amongst the tested configurations, the *ref*130 has the best performances at nergy range studied in this work. The combined effect of close DUs, denser local PMT distribution and slighlty larger bar size[1], along with still large instrumented volume grant the possibility to start studying Supersymmetric Dark Matter models with the future KM3NeT telescope since its first years of livetime.

[1] A fast analysis have been conducted on the same configuration with 6m bar lenght. The results, not shown here, show a small worsening of performance with the more compat bar, indicating that some investigations comparing string configuration versus large bar tower are to be taken.

7

Summary and Conclusions

The aim of this work was to study the performance of future KM3NeT detector to neutrino signals coming from WIMP annihilations in the Sun, by means of Monte Carlo analysis.

Dark Matter (DM) is still an open issue. Modern Cosmology and many observations suggest that the *dark* component of matter in the Universe is likely to be around 23%, and possibly constitued by non-relativistic Weakly Interacting Massive Particles (WIMPs). But no known particle is known to have the proper requirements. This opens the possibility of unknown physics beyond the Standard Model (SM) of Particle Physics.

One of the most appealing solution to the problem of the Dark Matter is given by Supersymmetry. Under certain assumptions, Supersymmetry elegantly provides a perfect WIMP (Weakly Interacting Massive Particle) candidate for DM. These Supersymmetric WIMPs can accumulate into dense object like planets, stars and heavier celestial bodies and thus undergo annihiliation to produce Standard Model particles, neutrinos included. This hypotesis can be verified thourgh direct and indirect experiments.

The basic idea of dark matter direct search is to detect the recoil energy of nuclei scattered off by WIMPs. The main contribution to the scattering process is due to the SI interaction, since heavy nuclei are usually used.

Indirect detection is based on the observation of particles emitted by WIMP annihilations. One of the methods is to use satellites in search for positrons, antiprotons, antideuterium and gamma excesses experiments.

Neutrino detection can prove to be a powerful tool too. We showed how these neutrino signals can be evaulated into modern km^3 Čerenkov neutrino telescopes and which limits can be posed on Supersymmetric DM with the future high energy neutrino underwater telescope KM3NeT.

To perform our MC analysis, a complex simulation chain developed by ANTARES Collaboration and modified by NEMO Collaboration has been used. In order to properly a generate neutrino flux from the Sun, part of the code has been subjected to further modifications, by adding new features which allow the generation of the Sun position in the detector's frame.

By using this tool, we compared three possible detector layouts for the future KM3NeT telescope.

The three layouts use the *tower* approach developed by the NEMO Collaboration and all are made of 154 Detecting Units. The different PMT distribution and instrumented volume reflect into different response at different energies.

A comparative analysis with special reference to low energy range has been conducted. Firstly, we compared the effective areas and the angular resolutions for the three configurations. We showed the the more compact one gains a sensitive boost in low energy range, without losing performance at higher energies, probably thanks to the new reconstruction strategy developed by the Collaboration, which is constantly evolving.

In order to evaluate the detector's response in three different configurations to neutrino signals coming from DM annihilations in the Sun, we used publicly available fluxes calculated with PYTHIA code as weight for our simulations.

So we studied the reconstructed events spectra with respect to the background, for selected models of DM, underlining important effects for the low energy range analysis.

We were able to calculate a sensitivity flux for these models and by that deriving limits on the rate of annihilation of DM inside the Sun.

Finally we showed some preliminary calculation on the WIMP Spin Dependent cross-section limit, which is a quantity that can be easily related to other (direct and indirect) experiments' results. The data are to be taken with prudence because the lack of muon backgorund statistics, but show that KM3NeT full detector will be able to reach IceCube sensitivity in the same years of data taking.

In any case the multiPMT and compact detector's layout proved to be the best solution amongst the tested ones, providng the best performances.

If confirmed, these results expose the outstanding KM3NeT detector's capability to detect low energy neutrino signals from DM annihilations into the Sun, and prove KM3NeT to be competitive with IceCube Experiment (with its low energy extenstion DeepCore) and with the next-generation direct search detectors like XENON 1T.

Further analysis on DM annihilating into the center of the Earth might provide unique insights on DM properties and are to be taken into consideration in a close future analysis.

Bibliography

[1] Zwicky F. *On the mass of nebulae and of clusters of nebulae* The Astrophysical Journal, 1937ApJ 3

[2] Rubin V. *Rotation of the Andromeda Nebula from a Spectroscopic Survey of Emission Regions*, Astrophysical Journal 159: 379 (1970) 4

[3] van Albada, T. S.; Bahcall, J. N.; Begeman, K.; Sancisi, R. *Distribution of dark matter in the spiral galaxy NGC 3198* Astrophysical Journal, Part 1 (ISSN 0004-637X), vol. 295, Aug. 15, 1985, p. 305-313.

[4] Lattuada D. *Studio della sensibilità del telescopio NEMO a neutrini di alta energia provenienti dalla sorgente estesa SNR RX J1713.7-3946*, Graduate Th. 60

[5] Marco Cirelli, Nicolao Fornengo, Teresa Montaruli, Igor Sokalski, Alessandro Strumia, Francesco Vissani *Spectra of neutrinos from dark matter annihilations* [arXiv:hep-ph/0506298v5] 19, 71, 76

[6] PYTHIA code WWW http://home.thep.lu.se/ torbjorn/pythiaaux/recent.html 19

[7] Braccesi A. *Dalle stelle all'universo. Lezioni di astrofisica* 2000, Zanichelli.

[8] Press & Schechter, 1974; Sheth et al., 2001; Jenkins et al., 2001; Springel et al., 2005 7

[9] http://people.roma2.infn.it/ dama/ 13

[10] Wilkinson Microwave Anisotropy Probe www http://map.gsfc.nasa.gov/ 8

[11] CoGeNT www http://cogent.pnnl.gov/ 13

[12] CRESST www http://www.cresst.de/ 13

[13] CDMS www http://cdms.berkeley.edu/ 13

[14] XENON www http://xenon.astro.columbia.edu/ 13

[15] PAMELA www http://pamela.roma2.infn.it/index.html 13

[16] FERMI Telescope www http://fermi.gsfc.nasa.gov/ 13

[17] CMS www http://cms.web.cern.ch/ 15

[18] ATLAS www http://atlas.web.cern.ch/ 15

[19] A.Morselli, B.Canadas, V.Vitale on behalf of the Fermi LAT collaboration *The Indirect Search for Dark Matter from the centre of the Galaxy with the Fermi LAT* arXiv:1012.2292v1 14

[20] Rizzo A. Search for neutralino dark matter with 6 years of data of the AMANDA-II neutrino telescope, PhD Th.

[21] Kopper C. Performance Studies for the KM3NeT Neutrino Telescope, PhD Th.

[22] Lim,G. Searching for Dark Matter with the Antares Neutrino Telescope, PhD th.

[23] Kelso C., Dan Hooper D., Buckley R. Toward A Consistent Picture For CRESST, CoGeNT and DAMA arXiv:1110.5338v1 12, 13

[24] Bertone, G. *Particle Dark Matter* Cambridge University Press.

[25] Gaisser T.K. *Cosmic Rays and Particle Physics*, FXXX Edition Cambridge University Press, 1990

[26] BAIKAL WWW *http://www.ifh.de/baikal/baikalhome.html*. BAIKAL Collaboration. 33

[27] NEMO WWW *http://nemoweb.lns.infn.it/*, NEMO Collaboration. 31, 35

[28] ANTARES WWW *http://antares.in2p3.fr/*, ANTARES Collaboration. 34, 35

[29] NESTOR WWW *http://www.nestor.org.gr/*, NESTOR Collaboration. 35

[30] AMANDA WWW *http://amanda.uci.edu/*, AMANDA Collaboration. 33

[31] IceCube WWW *http://icecube.wisc.edu/*, IceCube Neutrino Observatory. 33

[32] KM3NET WWW *http://www.km3net.org*, KM3NET Collaboration. 35

[33] AUGER WWW *http://www.auger.org/*, Pierre Auger Collaboration.

[34] Yu.A. Golfand and E.P. Likhtman, JETP Lett. 13 (1971) 323-326; A. Neveu and J.H. Schwartz, Nucl. Phys. B31 (1971) 86-112; A. Neveu and J.H. Schwartz, Phys. Rev. D4 (1971) 1109-1111; P. Ramond, Phys. Rev. D3 (1971) 2415-2418; D.V. Volkov and V.P. Akulov, Phys. Lett. B46 (1973) 109-130; J. Wess and B. Zumino, Phys. Lett. B49 (1974) 52-60; J. Wess and B. Zumino, Nucl. Phys. B70 (1974) 39-50

[35] H.E.S.S. WWW *http://www.mpi-hd.mpg.de/hfm/HESS/*, H.E.S.S. Collaboration. 14

[36] G. Riccobene et al., 2007. Astrop. Phys. vol. 27, 1. 31, 49

[37] The NEMO Collaboration. *Study and characterization of a deep sea site for a* km^3 *underwater neutrino telescope*. Report to ApPEC (2002), disponibile su http://nemoweb.lns.infn.it/siteport/.

[38] Migneco et al., *Status of NEMO*, 2006, NIM A 567, 444.

[39] P. Sapienza for NEMO Collaboration, Proc of VLVnT workshop, Amsterdam 2003, *www.vlvnt.nl/proceeding*.

[40] Y. Becherini for ANTARES Collaboration, 2006, NIM A 567, 477.

[41] G. Feldman, R. Cousins. *Unified approach to the classical statistical analysis of small signals*. 1998, Phys. Rev, Vol 57, 7. 41

[42] Trovato A. for KM3NeT Consortium, *Performance of the KM3NeT high-energy neutrino telescope* Il Nuovo Cimento, 34 (2011) Suppl. 1. 50

[43] LEPTO code www http://www.isv.uu.se/thep/lepto 45

[44] RSQ code, Giles David Barr. *The Separation of Signals and Background in a Nucleon Decay Experiment*. PhD thesis, University of Oxford, 1987. 45

[45] MUSIC code, P Antonioli, C Ghetti, E. V Korolkova, et al. *A three-dimensional code for muon propagation through the rock: MUSIC.* Astropart. Phys., 7:357, 1997 45

[46] G. Carminati, M. Bazzotti, S. Biagi, S. Cecchini, T. Chiarusi, A. Margiotta, M. Sioli, M. Spurio *MUPAGE: a fast atmospheric MUon GEnerator for neutrino telescopes based on PArametric formulas* 58

[47] Bugaev et al. *Atmospheric muon flux at sea level, underground, and underwater* 1998, Phys. Rev. D 58, 054001 58

[48] Boomerand www http://cmb.phys.cwru.edu/boomerang/ 8

[49] Okada A. *On the atmospheric muon energy spectrum in the deep ocean and its parameterization* 1994, Astrop. Phys. 2, 393-400

[50] Online Sun position calculator www.sunearthtools.com 61

[51] Heijboer, A. 2003. ANTARES Collaboration. Proc. 28th ICRC (Tsukuba, Japan), p. 1321.

[52] The Super-Kamiokande Collaboration: Y.Ashie et al, *Evidence for an oscillatory signature in atmospheric neutrino oscillation* 2004. Phys.Rev.Lett. 93, 101801.

[53] The KamLAND Collaboration, *Measurement of Neutrino Oscillation with KamLAND: Evidence of Spectral Distortion* 2005. Phys.Rev.Lett. 94, 081801.

[54] Gould A. *Cosmological density of WIMPs from solar and terrestrial annihilations* The Astrophysical Journal 1992ApJ 18, 76

[55] Halzen F., Hopper D., *Prospects For Detecting Dark Matter With Neutrino Telescopes In Light Of Recent Results From Direct Detection Experiments* Phys.Rev.D73:123507,2006 18, 76

[56] Abbasi R, et al for IceCube Collaboration *Limits on a muon flux from neutralino annihilations in the sun with the IceCube 22-string detector.* Phys Rev Lett. 2009 May 22;102(20):201302. Epub 2009 May 21. 78

[57] Christopher Wiebusch for the IceCube Collaboration *Physics Capabilities of the IceCube DeepCore Detector* arXiv:0907.2263v1 78

[58] G. Wikström and J. Edsjö *Limits on the WIMP-nucleon scattering cross-section from neutrino telescopes* arXiv:0903.2986v2

[59] G. Wikström *A search for solar dark matter with the IceCube neutrino telescope* PhD Thesis

[60] THE ICECUBE COLLABORATION *The IceCube Neutrino Observatory IV: Searches for Dark Matter and Exotic Particles* arXiv:1111.2738v1